Reduced Neuron-Specific Expression of the *TAF1* Gene Is Associated with X-Linked Dystonia-Parkinsonism

Satoshi Makino, Ryuji Kaji, Satoshi Ando, Maiko Tomizawa, Katsuhito Yasuno, Satoshi Goto, Shinnichi Matsumoto, Ma. Daisy Tabuena, Elma Maranon, Marita Dantes, Lillian V. Lee, Kazumasa Ogasawara, Ikuo Tooyama, Hiroyasu Akatsu, Masataka Nishimura, and Gen Tamiya

X-linked dystonia-parkinsonism (XDP) is a movement disorder endemic to the Philippines. The disease locus, *DYT3*, has been mapped to Xq13.1. In a search for the causative gene, we performed genomic sequencing analysis, followed by expression analysis of XDP brain tissues. We found a disease-specific SVA (short interspersed nuclear element, variable number of tandem repeats, and Alu composite) retrotransposon insertion in an intron of the TATA-binding protein-associated factor 1 gene (*TAF1*), which encodes the largest component of the TFIID complex, and significantly decreased expression levels of *TAF1* and the dopamine receptor D2 gene (*DRD2*) in the caudate nucleus. We also identified an abnormal pattern of DNA methylation in the retrotransposon in the genome from the patient's caudate, which could account for decreased expression of *TAF1*. Our findings suggest that the reduced neuron-specific expression of the *TAF1* gene is associated with XDP.

X-linked dystonia-parkinsonism (XDP [MIM314250]) is characterized by severe progressive torsion dystonia followed by parkinsonism.[1] Its prevalence is high (5.24 in 100,000) on Panay Island, Philippines.[2] Dystonia is a syndrome of sustained muscle contractions causing twisting and repetitive movements or abnormal postures,[3] and its pathogenetic basis is still unclear. XDP has a well-defined pathology of extensive neuronal loss and mosaic gliosis in the striatum (caudate nucleus and putamen),[4,5] which appears to resemble that in Huntington disease (MIM 143100). Identification of the disease gene of XDP may contribute to the elucidation of the molecular basis underlying not only XDP itself but also other diseases in which basal ganglia show neurodegeneration, such as Huntington disease and Parkinson disease.

A series of linkage analyses has mapped the disease locus, *DYT3*, to Xq13.1 (fig. 1).[6,7] A linkage disequilibrium study narrowed the *DYT3* locus to within a 350-kb interval on Xq13.1.[8] Subsequently, Nolte et al.[9] used PCR-based sequencing and screening analyses to report four SNPs and five disease-specific sequence changes (DSCs) in the "multiple transcript system" (*MTS*) within 260 kb of the *DYT3* region. However, PCR often fails to detect large sequence variants such as transposons. Moreover, the previous study of *MTS* did not include any brain specimens from patients with XDP. Therefore, the structure and expression of *MTS* transcripts are still unclear.

We performed the following studies to reveal the disease-causative gene of XDP. To find all disease-specific mutations within the *DYT3* region, we first performed genomic sequencing analysis to accurately determine the complete DNA sequence of this region. We also performed detailed expression analysis of the gene in brain specimens obtained from patients with XDP, because the expression of disease genes can be tissue specific. To determine the complete structure of the disease gene, we used a library consisting of "full-length" cDNAs frequently containing their 5′ ends.[10]

Material and Methods

Subjects and Samples

The study included 67 Filipino individuals (20 affected males) from 16 families residing in Panay. Information on all the patients is listed in table 1. All patients had the disease-specific haplotype between *DXS10017* and *DXS10018* in the *DYT3* region that had been defined elsewhere.[8,9] For construction of the BAC contig and portions of the RNA analysis, lymphoblastoid cells were immortalized by infection with the Epstein-Barr virus. This study involved a total of 137 healthy control subjects: 14 unrelated Filipinos, 44 Japanese, 38 African Americans, and 43 European Americans. Materials from the non-Filipino individuals were commercially provided by Coriell Cell Repositories. We used seven postmortem brains from seven male Filipino patients who had XDP. One of the seven brain specimens was frozen, and six were formalin fixed immediately at autopsy. The information on these seven patients with XDP is provided in table 2. We used the frozen brain from a single patient with XDP for long RT-PCR,

From the Department of Neurology and Neuroscience, University of Tokushima Graduate School of Medicine, Tokushima, Japan (S. Makino; R.K.; S.A.; S. Matsumoto; M.N.; G.T.); Department of Molecular Life Science, Tokai University School of Medicine, Kanagawa, Japan (S. Makino; S.A.; M.T.; K.Y.; G.T.); Department of Neurosurgery, Graduate School of Medical Sciences, Kumamoto University, Kumamoto, Japan (S.G.); Department of Internal Medicine, Section of Neurology, West Visayas State University Medical Center, Jaro, Iloilo, Panay, Philippines (M.D.T.; E.M.); Department of Health, Philippine Children's Medical Center, Quezon City, Philippines (M.D.; L.V.L.); Department of Pathology (K.O.) and Molecular Neuroscience Research Center (I.T.), Shiga University of Medical Science, Otsu, Japan; and Choju Medical Institute, Fukushimura Hospital, Toyohashi, Japan (H.A.)

Received August 21, 2006; accepted for publication December 13, 2006; electronically published January 23, 2007.

Address for correspondence and reprints: Dr. Gen Tamiya, Department of Neurology and Neuroscience, University of Tokushima Graduate School of Medicine, Tokushima 770-8503, Japan. E-mail: gtamiya@genetix-h.com

Am. J. Hum. Genet. 2007;80:393–406. 0002-9297/2007/8003-0002$15.00
DOI: 10.1086/512129

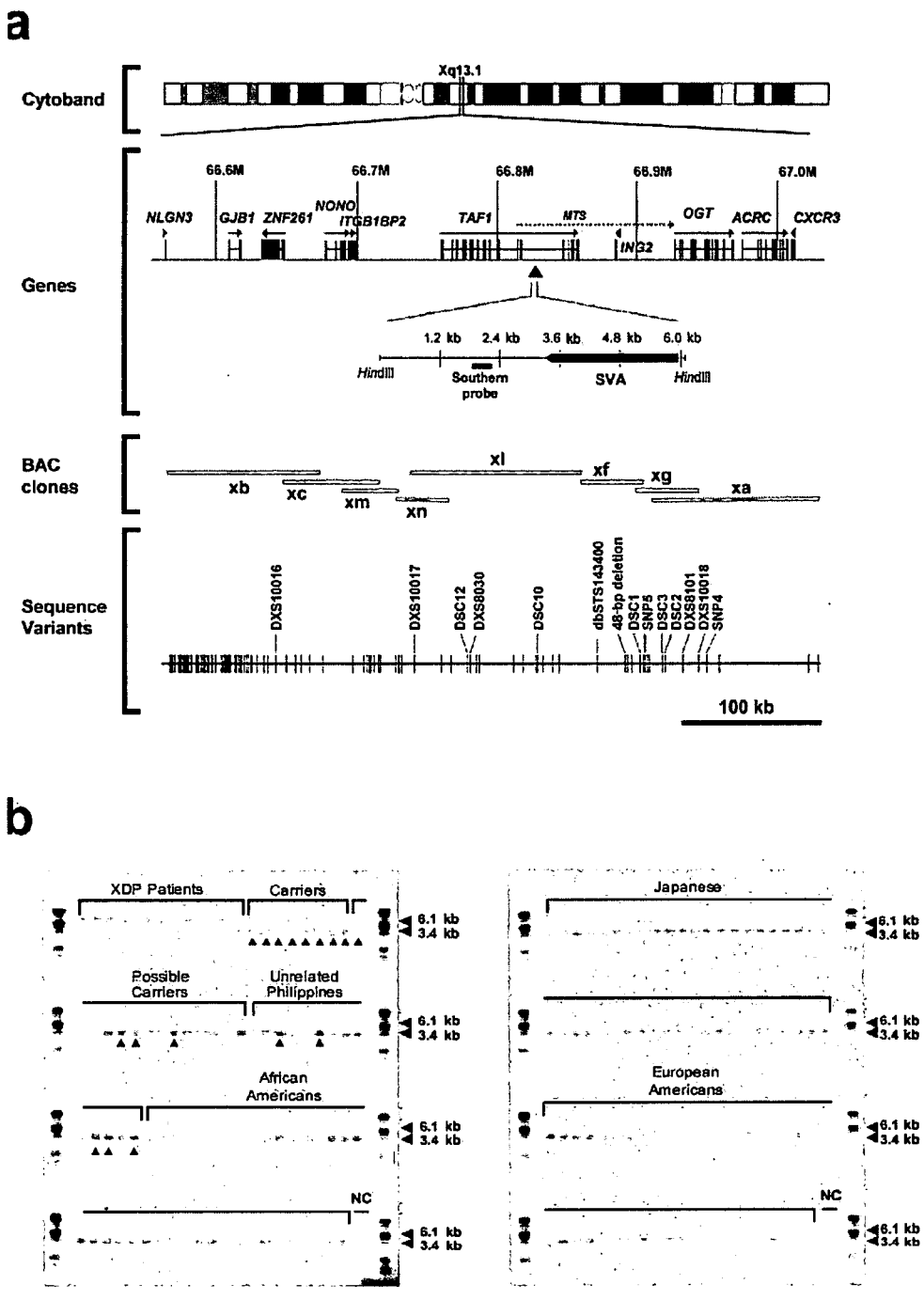

Figure 1. Genomic sequencing analysis of the *DYT3* region. *a*, Physical map of the *DYT3* critical region on Xq13.1. Annotated genes in this region that have experimentally verified coding sequences (and their proteins) include *NLGN3* (neuroligin 3), *GJB1* (gap junction protein, beta-1), *ZNF261* (zinc finger protein 261), *NONO* (non-POU domain–containing octamer-binding protein), *ITGB1BP2* (melusin [integrin beta-1 binding protein 2]), *TAF1* (TAF-250 [TATA-binding protein-associated factor, 250 kDa]), *ING2* (inhibitor of growth 2), *OGT* (O-linked N-acetylglucosamine transferase), *ACRC* (acid repeat–containing gene), and *CXCR3* (chemokine, CXC motif, receptor 3). The broken arrow indicates *MTS*. A unique Southern probe was designed for the *Hin*dIII-digested fragment containing the SVA retrotransposon insertion. Eight BAC clones comprising a continuous contig map cover 462,651 bp, from 66572462 to 67035112 in NCBI build 30. A total sequence length of 463,567 bp was determined, with 5.7-fold redundancy. Also shown is the distribution of 159 nucleotide variants that were identified by sequencing. None of these variants is located in any exon of these genes, including their alternative splicing forms. A red arrowhead indicates the SVA insertion. *b*, The SVA insertion in the XDP-related and healthy control populations. Information on the patients with XDP is given in table 1 (patients 1–13). The SVA insertion produces a 6.1-kb fragment, whereas the wild type produces a 3.4-kb fragment. Arrowheads in the gel indicate female individuals. Carriers are defined as mothers or daughters of patients with XDP. Possible carriers are daughters or sons of these carriers. NC = negative control.

Table 1. Information on All the Patients with XDP Who Were Studied by Southern Hybridization

Patient Number	Sample	Signal 6 kb	Signal 3 kb	Age at Onset (years)	Clinical Description
1	XD001	+	−	31	Generalized dystonia
2	XD002	+	−	38	Generalized dystonia
3	XD011	+	−	29	Muscle atrophy and generalized dystonia
4	XD013	+	−	45	No atrophy and dystonia
5	XD015	+	−	31	Limb atrophy and parkinsonism
6	XD024	+	−	41	Dystonia and parkinsonism
7	XD027	+	−	30	Dystonia and parkinsonism
8	XD028	+	−	30	Leg tremor and generalized dystonia
9	XD033	+	−	33	Parkinsonism (hand tremor)
10	XD036	+	−	50	Mild dystonia and parkinsonism
11	XD041	+	−	52	Dystonia and parkinsonism
12	XD054	+	−	30	Generalized dystonia
13	XD062	+	−	40	Severe atrophy
14	XD101	+	−	42	Swelling feet, difficulty walking, and sensory trick
15	XD103	+	−	46	Dystonia, parkinsonism, difficulty swallowing, and freezing gait
16	XD111	+	−	39	Dystonia, parkinsonism, and difficulty walking
17	XD112	+	−	33	Torticollis and parkinsonism
18	XD115	+	−	31	Jaw-opening dystonia and parkinsonism
19	XD131	+	−	36	Blephalospasm and writer's clamp
20	XD141	+	−	40	Cervical dystonia, axial dystonia, and parkinsonism

NOTE.—All patients are male. Plus sign (+) = presence of signal; minus sign (−) = absence of signal.

northern analysis, quantitative RT-PCR, and in situ hybridization. In addition, we used the six formalin-fixed brain specimens for immunohistochemical staining. This study complied with the ethical guidelines of the institutions involved.

Genome Analysis

We constructed two series of BAC libraries, using genomic DNA from a patient with XDP who was aged 41 years and had generalized torsion dystonia without parkinsonism. Cultured lymphoblastoid cells from a patient with XDP were embedded in agarose plugs, and then high–molecular-weight DNA was partially digested with *Eco*RI and was size fractionated by pulse-field gel electrophoresis. Size-fractionated DNA was cloned into the CopyControl pCC1BAC vector (Epicentre) and was transformed into DH10B cells by use of an electroporator. The same procedure was repeated with *Hin*dIII. We identified BACs covering the *DYT3* region by hybridizing ^{32}P-labeled PCR probes to filters generated from these BAC libraries. A shotgun library in pUC118 was constructed from each BAC clone. Cycle sequencing was performed using a BigDye Terminator v3.1 Cycle Sequencing kit (Applied Biosystems) and was analyzed on an ABI 3700 capillary sequencer. The gap clones were sequenced using a GPS-1 Genome Priming System (New England Biolabs). Raw sequence data were analyzed and assembled by ATGC software (Genetyx).

We digested 4 μg of genomic DNA in 300 μl of a standard reaction mixture containing 125 units of *Hin*dIII for 3 h at 37°C. For methylation detection, an aliquot of the *Hin*dIII-digested DNA was digested under the same conditions with a CpG methylase–sensitive enzyme, *Hpa*II. As a control reaction, an aliquot was also digested with *Msp*I, which is a CpG methylase–insensitive isoschizomer of *Hpa*II. After ethanol precipitation, the digested DNA was loaded onto a 0.8% agarose gel in 0.1 × Tris-borate-EDTA buffer for electrophoresis. After denaturation and the subsequent neutralization steps, the DNA was transferred to a positively charged nylon membrane (Roche Diagnostics). The filter was prehybridized for 1 h in DIG Easy Hyb buffer (Roche

Table 2. Information on All the Patients with XDP Who Were Studied by Expression Analysis

Patient Number	Age (years) At Onset	Age (years) At Death	Clinical Description	Cause of Death	Fixation	Examination(s)[a]
1[b]	42	52	Dystonia and parkinsonism	Pneumonia	Frozen; 4% paraformaldehyde	NB, LRT, QRT, ISH
2	40	54	Dystonia and parkinsonism	Pneumonia	Formalin	IHC
3	23	47	Dystonia and parkinsonism	Pneumonia	Formalin	IHC
4	56	59	Dystonia	Suicide	Formalin	IHC
5	38	52	Dystonia	Unknown	Formalin	IHC
6	35	42	Dystonia	Suicide	Formalin	IHC
7	34	46	Dystonia	Pneumonia	Formalin	IHC

NOTE.—All patients are male.

[a] IHC = immunohistochemical staining; ISH = in situ hybridization; LRT = long RT-PCR; NB = northern blot; QRT = quantitative RT-PCR.

[b] The results for patient 1 are presented in figures 2, 4, 5*a*–5*e*, 6, and 7.

Table 3. PCR Primer Sets for Fragment Amplification from the *TAF1* cDNAs

Fragment Name	Forward Primer			Reverse Primer			Amplicon Size (bp)
	Name[a]	Sequence (5′→3′)	T_m[b]	Name[a]	Sequence (5′→3′)	T_m[b]	
TA01	TAF_f_3	GGGAGCTCAGTAFAGTCACTTCTG	60.6	TAF_r_400	CCACCTCATTGATGTCTGAATAG	59.6	398
TA02	TAF_f_377	ACTAFTTCAGACATCAATGAGGTGG	60.4	TAF_r_772	TGGCATCATGCTGCATAATC	61.8	396
TA03	TAF_f_755	TTAFTGCAGCATGATGCCAC	60.4	TAF_r_1175	CCCAGCATATCATACCACAGTC	60.4	421
TA04	TAF_f_1152	CCGACTGTGGTAFTGATAFTGCTG	61.5	TAF_r_1550	CGTCCATATACCAGATCCTCATTG	62.7	399
TA05	TAF_f_1528	AATGAGGATCTGGTAFTAFTGGACG	60.2	TAF_r_1910	CGTAATTCCACAGCAGGAATTG	62.7	383
TA06	TAF_f_1889	CAATTCCTGCTGTGGAATTAFCG	62.7	TAF_r_2273	CCATATTTACAATCTGGTGCTCC	60.7	385
TA07	TAF_f_2251	GGAGCACCAGATTGTAFAATAFTGG	60.7	TAF_r_2598	TTCCATTCGTATCCTCCGTG	62	348
TA08	TAF_f_2580	ACGGAGGATAFCGAATGGAAG	60.1	TAF_r_2979	ATCTGCCACCCCAGTCAC	60.8	400
TA09	TAF_f_2945	GCAAGTGTCTGCTAFGAGGTGAC	60.3	TAF_r_3331	GTAGGTCAAAGATGCGCTGAC	61	387
TA10	TAF_f_3311	GTCAGCGCATCTTTGACCTAFC	61	TAF_r_3710	GTCCGTATGCGCACATAGG	61.3	400
TA11	TAF_f_3689	ATGCCTAFTGTGCGCATAFCG	61.8	TAF_r_4089	CAAGACAATTTTGGTCCCTTC	59.6	401
TA12	TAF_f_4069	GAAGGGACCAAAATTGTCTTG	59.6	TAF_r_4467	TAGCTCCAGATGCTCTCTGAAC	59.9	399
TA13	TAF_f_4413	CGTGCGTAFAACGCCTCTAFC	60.6	TAF_r_4808	CGACTCTGATACTTGTGCTTGG	61	396
TA14	TAF_f_4780	AACATCTCCAAGCACAAGTAFTCAG	60.7	TAF_r_5164	GCTTTTCTGGAGTGGCACTG	62.1	385
TA15	TAF_f_5130	TGTCTTGGATAFTTCCCAGTGC	61.1	TAF_r_5505	GTTGCTATCCTCCAAACCATG	60.5	376
TA16	TAF_f_5482	TCCCATGGTTTGGAGGATAFG	60.9	TAF_r_5862	AAGGCTAAGGTGTTAGTTAATTTCATG	60.3	381
TA17	TAF_f_5834	ATCATGAAATTAFACTAFACACCTTAFGCC	60.1	TAF_r_6231	TTAGTAGAGATGCGGTTTCGC	60.5	398
TA18	TAF_f_6073	GTAFACTTTAFTGTCCTCTTGATGTAFTTAFGG	59.1	TAF_r_6469	CAGGAGGGCTCTCATCTGC	62.3	397
TA19	TAF_f_6451	GCAGATGAGAGCCCTCCTG	62.3	TAF_r_6855	AAGGATCTGATAGAGTGCTTATCATG	60.2	405
TA20	TAF_f_6831	ATGATAFAGCACTCTAFTCAGATCCTTG	60.2	TAF_r_7164	CACACTCTGCCATTTCTAGACTG	60.1	334
TA21	TAF_f_7140	CACAGTCTAFGAAATGGCAGAGTG	60.1	TAF_r_7553	GGGTTATCATTGTGAACAGTTAGC	59.9	414
TA22	TAF_f_7277	GGCAGGAAGTAFTAFTCATCACAAGC	62.1	TAF_r_7606	CCAGCATACATAACAAACACAGAAG	60.9	330
MT23[c]	TAF_f_7277	GGCAGGAAGTAFTAFTCATCACAAGC	62.1	pMTS-r	GTGAGAGCTCAAAGACCAATAAG	58.3	779
Probe 1	TA_f_2333	TGCAAGCATTTGAGAACAACCT	62	TA_r_2690	GAGTCCATCCCTGTGCGTT	61.1	358
Probe 2	TA_f_4786	TCCAAGCACAAGTATCAGAGTCG	61.7	TA_r_5185	CTTCACCTTCCTGTGTTACCTGCT	63	400
Probe 3	TA_f_5637	GAGCGTACTAAGCCAGGTCCA	61.7	TA_r_6065	TTCATAATTTCCCCTCCTTCCC	62.4	393

NOTE—The PCR mixture contained 2 μl of the first-strand cDNA, 0.2 mM of each dNTP, 1 μM of each primer, 1× GeneAmp PCR buffer, and 2.5 units of AmpliTaq Gold DNA polymerase, in a 50-μl total volume. The PCR conditions were 9 min at 95°C, followed by 35 cycles at 95°C for 45 s, 60°C for 45 s, and 72°C for 60 s.

[a] The value in the third part of the primer name represents position in a major form of the *TAF1* transcript.

[b] T_m = annealing temperature (°C). The calculation conditions were 1,000 nM of each primer and 50 mM potassium ions.

[c] The primer set was used only for first-strand cDNA from *MTS*.

Table 4. Primers and Probes for the TaqMan Expression Assay

Assay Name	Primer Sequence (5′→3′)		Reporter 1 Sequence[a] (5′→3′)	Amplicon Size (bp)
	Forward	Reverse		
TAF1-5′	GACTGACGGTGCCTTGGT	GTCTGAATAGTCCACAGCATCTTCT	ACCCACCCTTCATCATTT	70
TAF1-3′	ACCTTATTCTGGCCAACAGTGTT	ACAATCTCCTGGGCAGTCTTAGTAT	ACTCTCAGGTCCATTATAC	73
TA02-334	TGGGACCAATGAAGAAGGATAAGGA	ATTCTGAGTCAGAGGAACTACTGAAGT	CCACTTTCTCACCAGTAATAG	81
TA08-269	CTCTGCGCTGACTTCAAACG	TTCCTCATTTTCTTCTTCTGGAGCAA	CCATAGCCAGCATCCTGT	79
TA09-391	GTGGTGAAGGATTCTCCTATGTGAA	ATCTGTTCCTGTCACTGTCTTCTTC	CAGCAGAAGGTAGGATGATAA	105
TA09-693	TGCCAAGCAACTTCTACGTAAATTTG	TCCAACTCTATACAAAGCCCCTAGT	CACACTCACCCTCTTCC	99
TA14-317	ACCTTATTCTGGCCAACAGTGTT	CCTCCAAAGCTGCTTCTTTAGCA	TTGAGTCAAATGTTCATCATACATT	97
TA14-389	GGAGATTGTGAACGTCTGTTACCA	TCCTTCTCAAGTTGAGTCAAATGTTCAT	CATACTACCTCAGTCAATGTC	73
TA14-391	CCCCAGGGCCCTACAC	CTGAGGGATGTGTTGGTATCATACAA	CCTCAGGCTAAGCCTC	64
TA14-407	GGGAGAGCTTTCTGGATGATGTAAA	ACAATCTCCTGGGCAGTCTTAGTAT	CTGACTCTCAGGTCCTGCACG	119
TA15-477	AGTGCCACTCCAGAAAAGCA	CCTCGCCCAGCCTACCT	CCTGGCGCATCTGTGT	61
TA18-261	GTGGCTCACACCTGTAATCTCA	CCTCCCGGGTTCAAGTAATTCTC	CAGCCTCCCAGAGTGC	67
TA14-385N[b]	CCCCAGGGCCCTACAC	CTGAGGGATGTGTTGGTATCATACAA	CCTCAGCCTCCTGATT	58
TAF1-M	GCTAAAGCTCTGCGCTGACT	TTAAGCACCCACCAGTTTGAGT	CATCCCTGTGCGTTTGA	60
TAF1-3′N	CCCAGTGCCACTCCAGAAAA	CAGTTCCTTCCTCTTCATCTGCAA	ACCTTCCTGTGTTACCTGC	82
MTS-V4	TTGCTCTTGGGCTCTGCATT	CTGGCACGGATTTTCACTATCTT	ACTCCTTACAGGTACCAATGA	251
MTS-37/1	CCCATGGTTTGGAGGATAGCA	CATCTCTGAATGGCTTGTTCATTG	TCAGGTGATGAACTTCAATA	166
MTS-37/3	CCCATGGTTTGGAGGATAGCA	TCGTTGCTCCAGAGATCTTTGTG	ACATCAGGTACCAATGAAC	83
MTS-2/3	GGCCTCCGGCATTGCT	TCGTTGCTCCAGAGATCTTTGTG	TCCACTGTACCAATGAA	112
MTS-32′/34′	CAACAGTGTTAAGTATAATGGGTACATGTG	CTGAGGGATGTGTTGGTATCATACAA	TCAGGCTAAGCCTCCT	268
MTS-3/4	GTGTCCGGAGTTGGTTCCT	TGGCACGGATTTTCACTATCTTCA	CCTTCGCGCTTCAGGC	105

[a] For the reporter 1 sequences, the dye was FAM.

[b] This probe is designed to detect all isoform sequences not containing exon 34′.

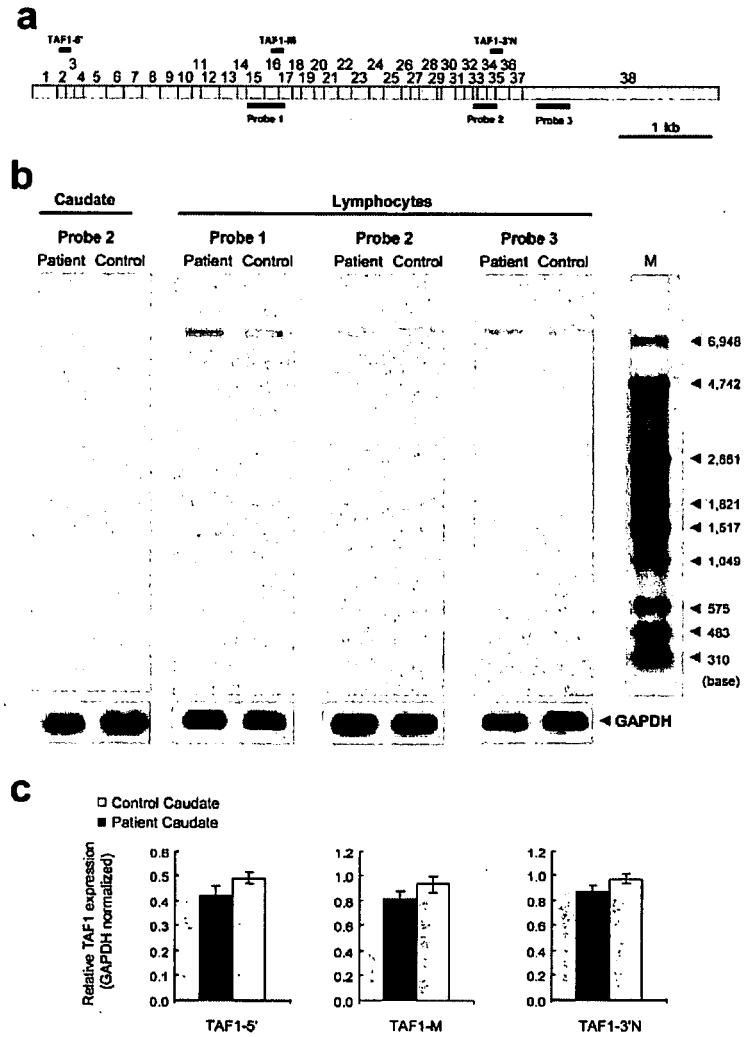

Figure 2. Northern analysis. *a*, Three probes for northern hybridization to *TAF1* (detailed information on these probes is given in table 3). *b*, Total RNA samples from the caudate and lymphoblastoid tissues. The hybridization signal seen at ~7 kb, which represents *TAF1*, was observed in every lane, but a signal was never seen at the smaller sizes corresponding to *MTS* transcripts reported elsewhere. This result suggests that the sequences of TAF1 isoforms have such small differences in size, probably less than a few hundred base pairs, that standard northern analysis cannot discriminate between them in 1% agarose gels denatured by 2% formaldehyde. A probe for *GAPDH* was also hybridized to each membrane as a loading control. M = DIG-labeled molecular-weight marker. *c*, Relative *TAF1* expression. The hybridization signal seen at ~7 kb, representing *TAF1*, had a tendency toward slight reduction in patient caudate, so, to confirm this, TaqMan assays were performed.

Diagnostics) and then was hybridized overnight (16–18 h) at 40°C. The PCR probe was amplified using primers XD_probe-F (5′-AGCTTTGCTGCCATTG-3′) and XD_probe-R (5′-AAGACCCTTATTATTCATGAGTG-3′). After washing the filter for 30 min at 68°C in DIG Wash and Block buffer, drops of 1/100-diluted disodium 3-(4-methoxyspiro {1,2-dioxetane-3,2′-(5′-chloro) tricyclo [3.3.1.1^{3,7}]decan}-4-yl) phenyl phosphate (CSPD [Roche Diagnostics]) were added and the filter was exposed to x-ray film for 1–5 h.

Table 5. All Nucleotide Variants in the *DYT3* Critical Region on Xq13.1

The table is available in its entirety in the online edition of *The American Journal of Human Genetics*.

RNA Isolation

Total RNA was isolated from caudate, cortex, and accumbens of a frozen brain by use of an RNeasy Lipid Tissue Midi kit (QIAGEN) with a DNaseI treatment step, after homogenization with a Polytron PT1300D (Kinematica). Total RNA from lymphoblastoid cell lines was also isolated by the same procedure. RNA sources from six Japanese brains were used as neurologically healthy con-

trols by the same procedure. Also, two commercial human brain RNA sources were used as controls—cerebral cortex total RNA (catalog number 636561) and caudate nucleus total RNA (63566)—along with human tissue total RNA sources from heart (64100), spleen (64093), lung (64092), liver (64099), and thymus (64107), provided by BD Bioscience Clontech, and stomach (735038), provided by Stratagene. The quality and quantity of total RNAs were assessed using an Agilent 2100 Bioanalyzer (Agilent). The 2:1 ratio of 28S:18S rRNA was employed as a threshold for intact RNA. The quantity was confirmed by the RiboGreen RNA fluorescence assay (Molecular Probes).

Northern Analysis

For synthesis of riboprobes, we performed PCR and cloning into the TA-vector (Promega), using the three primer sets in table 3: TA_f_2333 and TA_r_2690 for probe 1, TA_f_4786 and TA_r_5185 for probe 2, and TA_f_5637 and TA_r_6065 for probe 3. Total RNA samples of 10 μg were loaded into a 1% agarose gel denatured by 2% formaldehyde gel. The gel was run in 1 × 3[N-Morpholino]propanesulfonic acid buffer. After electrophoresis, the RNA was transferred to a positively charged nylon membrane. After prehybridization for 1 h in DIG Easy Hyb buffer at 68°C, hybridization was performed overnight (16–18 h) at 68°C. The filters were washed twice for 5 min with 100 ml of 2 × saline sodium citrate (SSC) and 0.1% SDS at room temperature and then were washed twice for 15 min with 0.1 × SSC and 0.1% SDS at 68°C. We employed the standard conditions and procedure provided by Roche Diagnostics.

Long RT-PCR Analysis

Long RT-PCR analysis was performed in two steps: (1) first-strand synthesis from RNAs of the control and XDP caudates by long reverse transcription (RT) and (2) fragment PCR by use of the long RT products (i.e., cDNA) as a template. Such a long RT-PCR method is known to be effective for defining the extent of a large transcript.[11] The two parts revealed not only the extent of the transcripts but also alternative exons included in the transcripts. Long RT was performed using TAF_r_7621 for the TATA-binding protein-associated factor 1 gene (*TAF1* [MIM 313650]) and MTS_r for *MTS* as the long RT primer.

Quantitative RT-PCR

cDNA was synthesized from the total RNA by use of random hexamers with a TaqMan Reverse Transcription Reagents kit (Applied Biosystems). All the primers and probes are listed in table 4. We also employed a control probe for 18S rRNA (4319413E) and the glyceraldehyde-3-phosphate dehydrogenase gene (*GAPDH*) (4310884E) and examined a probe for the dopamine receptor D2 gene (*DRD2*) (Hs00156514_m1). We used a final concentration of 250 nM probe, 900 nM primers, and 50 ng cDNA in a 50-μl reaction volume in a 96-well reaction plate on an ABI PRISM 7000 in accordance with the standard procedure. The conditions of real-time PCR consisted of a holding step for 2 min at 50°C and 1 min at 95°C followed by 50 cycles for 15 s at 95°C and 1 min at 60°C. Quantity was calculated every time by use of a standard curve for each well. All quantitative data normalized by adjustment for 18S rRNA were tested by Smirnov's test with

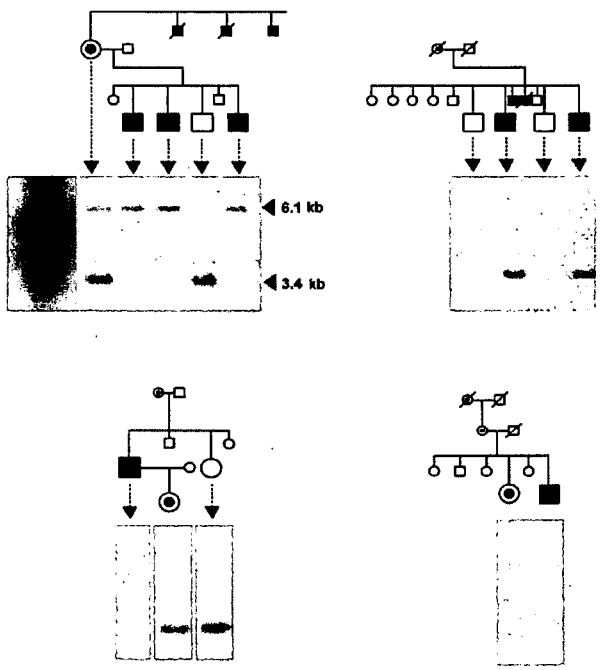

Figure 3. The SVA insertion in an additional seven patients with XDP and their relatives, from four families. Information on these patients is given in table 1 (patients 14–20).

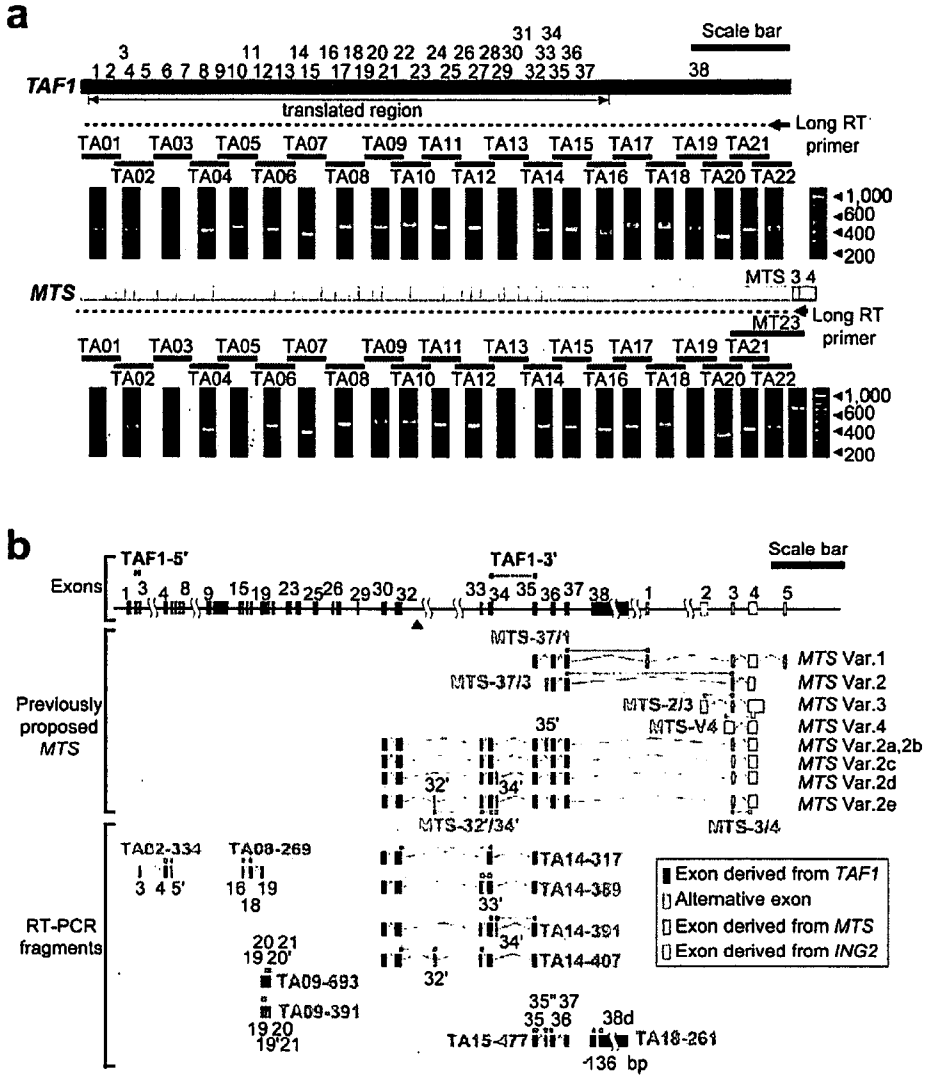

Figure 4. Long RT-PCR and the alternative exons of *TAF1*. *a*, Long RT-PCR analysis. The broken line indicates an expected cDNA fragment of *TAF1* with the long RT primer on the end of exon 38 (*short arrow*). By subsequent PCR with the use of the long cDNA, six lanes—TA02, TA08, TA09, TA14, TA15, and TA18 (*red bars*)—showed multiple bands. Other lanes (*black bars*) contained single bands. Also shown is the result obtained using the *MTS*-specific long RT primer on its 3′ end. There was no difference between the *TAF1* and *MTS* primers or between the patient and the control results (patient data not shown). Scale bar = 1 kb. *b*, Ten alternative exons, including two exon skippings and one deletion, were identified by RT-PCR. The detailed sequence information for these exons is annotated in our AB191243 deposition in DNA Databank of Japan (DDBJ). Of 10 alternative exons, 3 were reported elsewhere as exons of *MTS*, but a form including both exon 32′ and exon 34′ was not detected. For quantitative RT-PCR, 17 TaqMan probes were designed. Two TAF-series probes (*red*) and 10 TA-series probes (*pink*) were designed to detect mainly the TAF1 common forms and alternative splicing isoforms, respectively. The other five MTS-series probes (*orange*) were designed to detect the *MTS* transcripts reported elsewhere. Var. = variant. Scale bar = 5 kb.

a 5% significance level. We used Student's *t* test to test the difference in means of the expression levels between patients with XDP and healthy control caudate nuclei, after checking the acceptance of the quality of variances between the two groups by the *F* test.

In Situ Hybridization

Synthesis of DIG-labeled riboprobes for *TAF1* (probe 3 in fig. 2*a*), as well as for β-actin (*ACTB*) and glial fibrillary acidic protein (*GFAP*) as controls, was performed according to the procedure

Table 6. Linearity of Amplification Curve from Threshold Cycle (Ct) = 25 to Ct = 35

Assay	Slope (SD)	r (SD)	r^2 (SD)
MTS-37/1	.0020 (.0032)	.31 (.641)	.48 (.226)
MTS-37/3	.035 (.0123)	.82 (.036)	.68 (.061)
MTS-V4	.011 (.0098)	.51 (.422)	.43 (.285)
MTS-2/3	.00016 (.0014)	−.10 (.580)	.32 (.213)
MTS-32′/34′	.00073 (.0005)	.77 (.258)	.65 (.292)
MTS-3/4	.054 (.0351)	.81 (.017)	.66 (.032)
TA14-385N[a]	1.37 (.0424)	.99 (.002)	.97 (.004)

NOTE.—Slopes of the resulting lines, correlation coefficient (r) values, and coefficient of determination (r^2) values were calculated by curve-fitting with linear function against normalized reporter signal (ΔRn) values from Ct = 25 to Ct = 35 in each amplification curve of the real-time PCRs. We employed the threshold with slope >0.5 and $r^2 > 0.6$.

[a] The TaqMan probe was employed as a positive control to show standard amplification and linearity from Ct = 25 to Ct = 35.

used for northern analysis. The caudate blocks were fixed with 4% paraformaldehyde. After cryoprotection, serial 20-μm sections were cut in a cryostat. The sections were reacted with alkaline phosphatase–labeled anti-DIG antibody (diluted 1:200 [Roche Diagnostics]) in 1% skim milk in sodium Tris (hydroxymethyl)-aminomethane (NT) buffer. After washing with NT buffer, the positive signals were detected by nitroblue tetrazolium chloride (Roche Diagnostics) and 187 μg/ml 5-bromo-4-chloro-3-indolylphosphate (Roche Diagnostics).

Immunohistochemical Staining

The six tissues from six different patients with XDP were fixed in 10% neutral formalin, were sliced, and were embedded in paraffin, and 3-μm sections were cut on a microtome and were mounted on Matsunami adhesive silane–coated glass slides. After routine deparaffinization, rehydration, and blocking of endogenous peroxidase activity, all sections were processed for microwave-enhanced antigen retrieval. The sections were blocked with 3% BSA in PBS (pH 7.2) for 1 h and then were incubated overnight at room temperature in 3% BSA-PBS containing goat polyclonal antibody against *TAF1* (diluted 1:5,000 [Santa Cruz]). Rabbit polyclonal antibody against *GFAP* (Dako) was also used as a control. For the visualization of bound antibodies, we used Histofine Simplestain Max-PO (G) (Nichirei) and the liquid diaminobenzidine (DAB) substrate chromogen system (Dako Cytomation). The sections were further processed for enhancement of the DAB reaction products by use of a Dako Envision Kit (Dako Cytomation).

Full-Length Cloning and Direct Sequencing of the TA14_391 Isoform

To determine the full-length TAF1 isoform, including the 5′ end of the transcript, a CapSite cDNA library derived from human brain (317-04041 [Nippon Gene]) was used. The CapSite cDNA libraries consist of cDNAs in which the 5′ cap structure (m7Gppp) of eukaryotic mRNA is replaced with a synthetic oligoribonucleotide to label the 5′ end of the cDNA, enabling identification of the 5′ end sequence by PCR.[10] For amplification of the 3′ end, a whole Marathon-Ready cDNA library derived from human brain (BD Biosciences Clontech) was used. The reaction mixture contained 1 μl of the library, 200 mM of each primer, 0.16 mM of each deoxyribonucleotide diphosphate (dNTP), 1× BD Advantages2 PCR buffer, and 1× BD Advantages2 Polymerase Mix (639300 [BD Biosciences Clontech]) in a total volume of 50 μl. The PCR consisted of denaturation for 30 s at 94°C, followed by 5 cycles for 5 s at 94°C and 10 min at 70°C and then 20 cycles for 5 s at 94°C and 10 min at 78°C. An aliquot of the first PCR product was used for the second PCR reaction under the same conditions as the first-round PCR but with different primers. We used a primer set for the first PCR—first RDT primer (Nippon Gene) and TA3_r_5070 (5′-GGTATCATACAAATCAGGAGGCTT-3′)—and then used a set for the second heminested PCR—second primer and TA3_r_5070. These primers were purified by PAGE extraction. Alternative exon 34′–specific primers were designed to prevent erroneous amplification due to PCR slippage. For amplification of the 3′ end, a whole Marathon-Ready cDNA library derived from human brain (BD Biosciences Clontech) was used along with the primer set TA6_f_5032 (5′-CCCTACACGCCTCAGGCTA-3′) and TA2_r_7606 (5′-CCAGCATACATAACAAACACAGAAG-3′) under the same conditions as those used for the CapSite cDNA but as a single PCR reaction. Direct sequencing was done on these PCR products. After purification by a PCR Product Pre-Sequencing kit, cycle sequencing was performed using a BigDye Terminator v3.1 Cycle Sequencing kit, with 20 internal primers for a second PCR product from CapSite cDNA and 8 internal primers for the PCR product from Marathon-Ready cDNA. Direct sequencing was done on two long PCR products by use of the following primers: TAF_f_377, TAF_f_755, TAF_f_1152, TAF_f_1528, TAF_f_1889, TAF_f_2580, TAF_f_2945, TAF_f_3311, TAF_f_3689, TAF_f_4069, TAF_f_4413, TAF_f_4780, TAF_r_2273, TAF_r_2598, TAF_r_2979, TAF_r_3331, TAF_r_5164, TAF_r_5505, TAF_r_5862, TAF_r_6231, TAF_r_6469, TAF_r_6855, TAF_r_7164, TAF_r_7553, and TAF_r_7606 (table 3).

Results

Entire Genomic Sequence of the DYT3 *Region*

Two series of BAC libraries were constructed using DNA from a patient with XDP who had a disease-specific haplotype[8,9] in the *DYT3* region. From these libraries, a continuous BAC contig consisting of eight BAC clones was then generated to cover the *DYT3* region between the *GJB1* and *CXCR3* genes (fig. 1*a*). By applying a shotgun sequencing strategy, we accurately determined the complete DNA sequence of the BAC contig, with 5.7-fold redundancy. The total sequence length of the BAC contig was 463,567 bp. A comparison between our sequence from the patient with XDP and a reference sequence from National Center for Biotechnology Information (NCBI) build 30 showed a total of 159 sequence variants: 89 single-nucleotide substitutions, 68 small insertions/deletions (indels), 1 retrotransposal insertion, and 1 large (1,666-bp) deletion (all variants are listed in table 5). Of these variants, 53 were known SNPs, comprising 50 substitutions and 3 indels. Of the 68 indels, 62 were repetitive units of STRs, and the other 6 indels were also located in certain types of STRs. The large deletion was a direct repeat sequence spanning 1,666 bp. The retrotransposal insertion in intron 32 of the *TAF1* gene (fig. 1*a*) was 2,627 bp in length, which is categorized as an SVA (short interspersed nuclear element, VNTR, and Alu composite) retrotransposon.[12,13] The SVA retrotransposon insertion in the *DYT3* region had been never reported. However, none of these

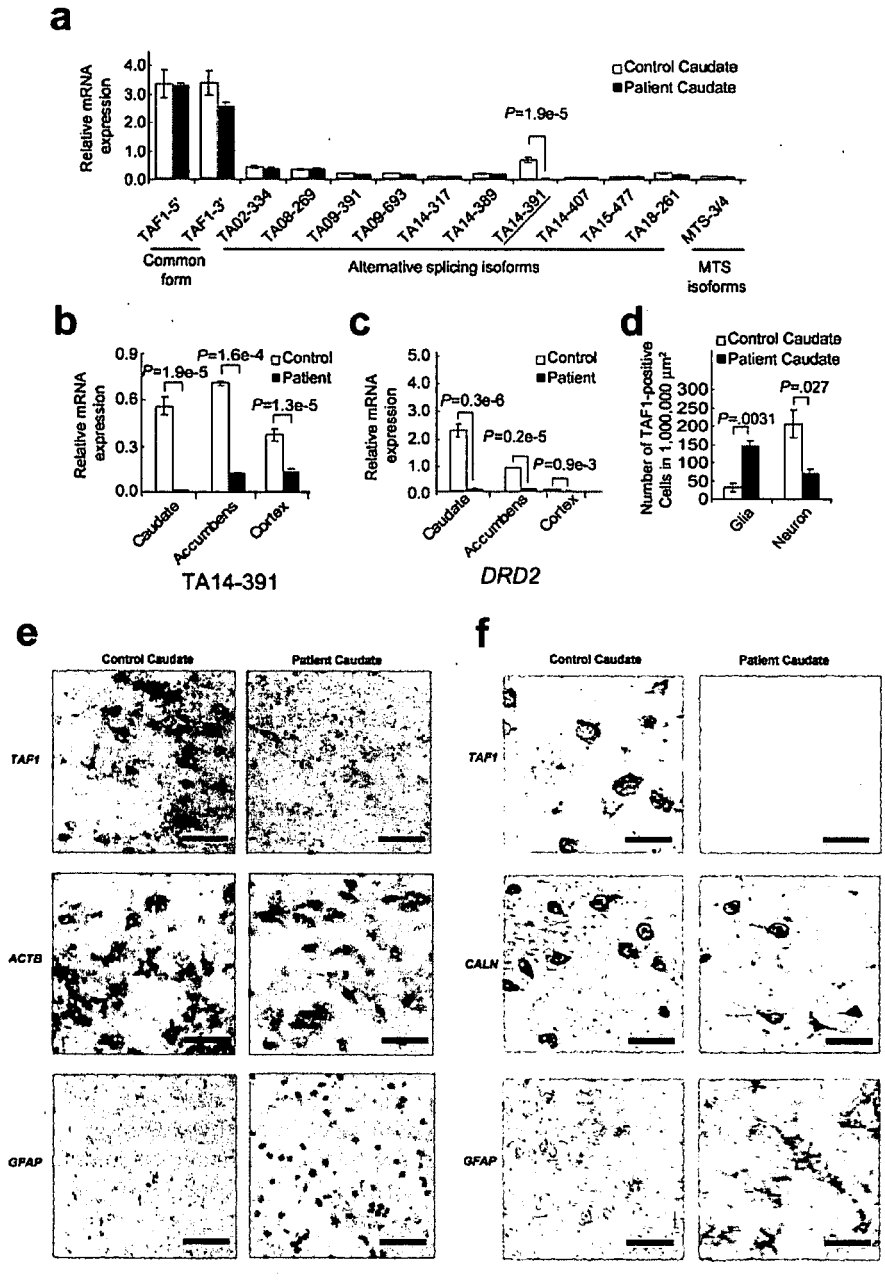

Figure 5. Expression of the TAF1 isoforms in the caudate. *a,* Expressions are shown relative to the expression of 18S rRNA (as an internal control). The label "relative mRNA expression" means relative mRNA expression level to 1/20 × 18S rRNA. Values are expressed as means ± SEM ($n = 3$). The TA14-391 probe showed a significant reduction in the patient's caudate. Two-sided *P* values are shown. Also shown is the expression level of TA14-391 (*b*) and *DRD2* (*c*) in three brain regions: caudate, accumbens, and cortex. All regions showed a significant decrease in TA14-391 expression. *d,* Morphometry analysis of *TAF1*-positive cells in XDP and control caudate nuclei. The number of each type of cell was counted in 1,000,000-μm^2 areas of the caudate nuclei. These were gliosis and neuronal loss in the XDP caudate nucleus. *e,* In situ hybridization analysis of *TAF1*. Although many *TAF1*-positive neurons were observed in both tissues, the expression level was apparently low in the patient's caudate neurons, even when a common probe for exon 38 was used. By contrast, the expression level of *TAF1* in glial cells was weak in both tissues. ACTB = β-actin; GFAP = glial fibrillary acidic protein. Strong *ACTB* signals were shown in glial and neuronal cells. The *GFAP* probe stains active glial cells, especially in the XDP caudate nucleus, because of activation by astrogliosis. In contrast, we observed no signal when using sense probes of these genes (data not shown). Scale bar = 25 μm. *f,* TAF1 immunohistochemical staining. Nearby sections were stained with polyclonal antibodies against TAF1, calcineurin (CALN), and GFAP. The immunoreactivity of TAF1 in the XDP caudate neurons was apparently weak. Moreover, the immunoreactivity of TAF1 in glial cells was originally weak in both tissues. Similar immunoreactivity was observed in three other brain tissues from three different patients with XDP. Scale bar = 25 μm.

Table 7. Abundance of the Probe TA14-391 in Various Tissues and Cell Lines

Tissue or Cell Line	Mean (SE) [10^{-5} fmol per 100 ng RNA]	
	TA14-391	TAF1 Major Form
Lymphocytes	0	3.68 (.08897)
Heart	0	.0873 (.00484)
Spleen	0	3.13 (.06749)
Lung	0	.133 (.00536)
Liver	0	4.20 (.21582)
Thymus	0	1.44 (.07147)
Stomach	0	1.23 (.03865)
Caudate	.699 (.00761)	3.30 (.50351)
Cortex	.463 (.00308)	3.70 (.57268)
Neuroblastoma, SH-SY5Y	.213 (.00694)	4.68 (.55110)
Glioblastoma, HTB15	0	1.67 (.44595)

NOTE.—The abundances for TA14-391 and the TAF1 major form (TA14-385N) were determined using quantitative RT-PCR by use of each clone of known concentration in the plasmid as an internal control.

variants was located in any exon or promoter of the annotated genes that have experimentally verified coding sequences, including their alternative splicing exons. In the region between *DXS10017* and *DXS10018*, there were 25 variants, which included the SVA insertion and the 1,666-bp deletion. We confirmed these variants in an ethnic panel (see the "Material and Methods" section) that included patients with XDP who have the disease-specific haplotype. DSCs 12, 10, 1, 3, and 2 were disease-specific among patients with XDP tested here as well as in a previous report.[9] The 1,666-bp deletion was detected by PCR among all affected and unaffected Filipinos and in the ethnic panels (data not shown) and was considered to be nonspecific. By contrast, the SVA retrotransposon was clearly disease specific in our data set (figs. 1*b* and 3). These disease-specific variants, the DSCs and the SVA retrotransposon, were located around the *TAF1* and *MTS* genes.

Previously Proposed MTS *Transcripts*

Next, northern hybridization and long RT-PCR analysis were undertaken to confirm the structures and expression of the *TAF1* and *MTS* genes. Northern analysis showed that the hybridization signal seen at ~7 kb of *TAF1* had a tendency toward reduction in patient caudate and that the *MTS* transcript lengths reported elsewhere[9] were not detectable in RNAs from either patient or control tissues (fig. 2*b*). Long RT-PCR analysis showed that the PCR fragment pattern from *MTS* was identical to that from *TAF1* (fig. 4*a*). If the *MTS* transcripts had lacked upstream exons 1–29 and exon 38, spanning >2 kb, as shown in the previous report,[9] the northern analysis would have detected the corresponding signals at ~2–5 kb. Moreover, our long RT-PCR analysis showed that exons 3 and 4 from *MTS* (gray exons in fig. 4*b*) are attached at the 3′ end of exon 38 of *TAF1*. Quantitative RT-PCR analysis by the TaqMan assay with five probes designed to detect the previously proposed *MTS* transcripts MTS-V4—which was regarded as a candidate transcript for *DYT3* because of a deduced amino-acid change[9]—MTS-37/1, MTS-37/3, MTS-2/3, and MTS-32′/34′ (fig. 4*b*) yielded very weak and irregular amplification signals that did not allow quantification of expression levels in the caudate nucleus (table 6), whereas the probe MTS-3/4 for exons 3 and 4 attached to *TAF1* yielded a relatively weak but regular signal (table 6). These results consistently suggested that the previously proposed *MTS* transcripts may be extremely rare or unexpressed and that at least exons 3 and 4 of *MTS* may be just an additional part of the 3′ UTR of *TAF1*, rather than part of a new distinct short gene.

Decreased Expression of TAF1 *in the XDP Brain*

At least 10 new alternative splicing exons around *TAF1* were found by long RT-PCR analysis (fig. 4*b*), but neither the DSCs nor the SVA insertion were located in any known and predictably translated regions of the *TAF1* exons. We then examined the expression levels of various forms of *TAF1* in the XDP caudate nucleus, using quantitative RT-PCR by designing specific probes for the TaqMan assay (fig. 5*a*). One of these probes, TA14-391—with an alternative exon of 6 additional bp, named "exon 34′"—showed a highly significant decrease in its expression level in the caudate nucleus of the patient with XDP (fig. 5*a*), which was less than ~1/40 of that in the normal control, and its expression was virtually limited to brain and neurons (table 7). TA14-391 was the second-most abundant among all *TAF1* species (fig. 5*a*), and its expression level in the control caudate nucleus was 1/4–1/5 of that of the major form of *TAF1* (table 7). TA14-391 also showed a significantly decreased level of expression in the cortex and the nucleus accumbens of the patient with XDP (fig. 5*b*), although these regions had no neuronal loss. These findings suggest that the decreased level of expression was the cause rather than the result of neuronal loss in the caudate nucleus of the patient with XDP. In addition to the TaqMan assay, in situ hybridization was performed in the caudate by use of a riboprobe common to TAF1 isoforms that are located in exon 38 (probe 3 in fig. 2*a*). The riboprobe showed decreased expression in the caudate neurons of the patient, although the weak expression was still present in glial cells (fig. 5*e*). Immunohistochemical examination by use of a polyclonal antibody against the common epitopes of *TAF1* also showed decreased immunoreactivity in the XDP neurons in the caudate nucleus from other patients with XDP (fig. 5*f*). These findings suggest that the deficiency of the neuron-specific isoform of TAF1, TA14-391, reflects these histologically verified neuron-specific decreases of *TAF1* expression and that TA14-391 is one of the neuron-specific isoforms, whereas apparently similar levels of mRNA expression for TAF1 or its isoforms as a whole (figs. 2*b*, 2*c*, and 5*a*) can be accounted for by increased glial expression of *TAF1* due to intensive astrogliosis[4,5] (fig. 5*d*–5*f*), obscuring the decreased expression in neurons. The TA14-391 isoform may

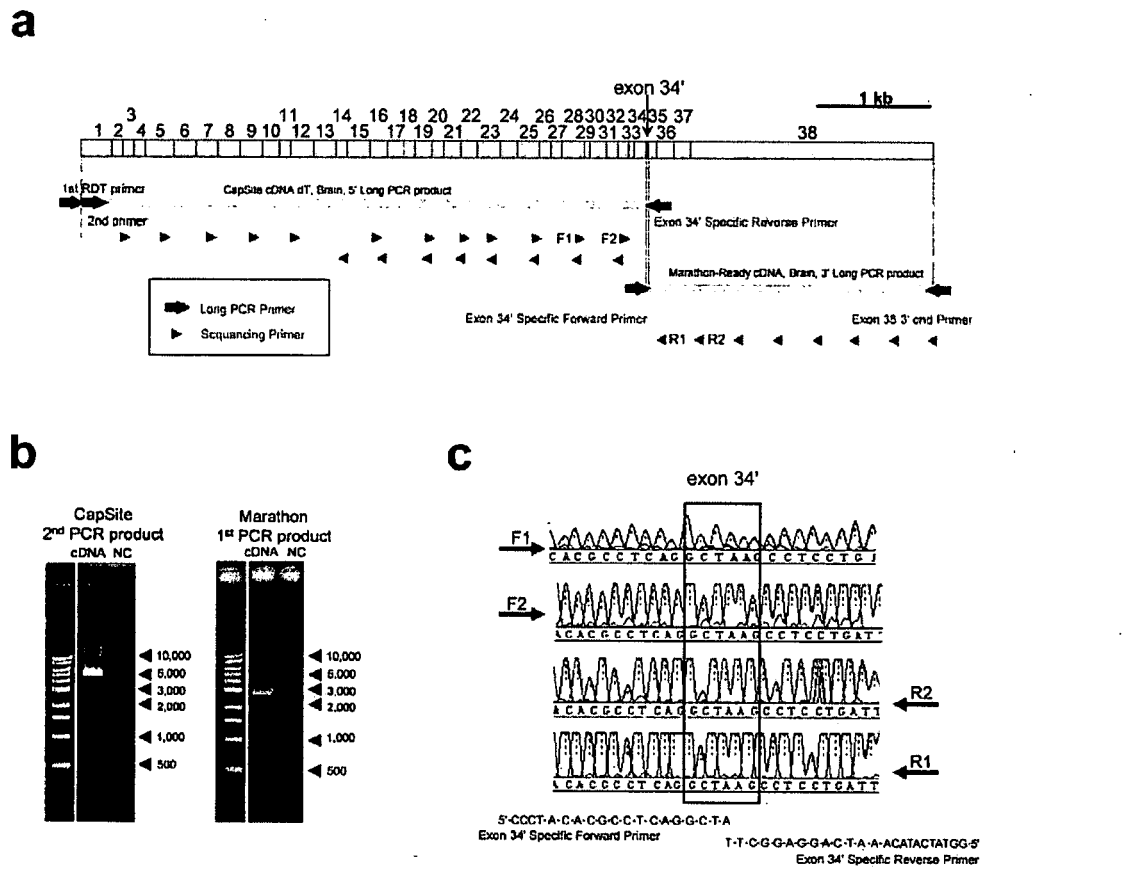

Figure 6. *a*, Full-length cloning of a TAF1 isoform sequence containing alternative exon 34′. The 5′ end was obtained from CapSite cDNA from brain. The 3′ end was obtained from Marathon-Ready cDNA from brain. The complete DNA sequences of these long products were determined by a PCR direct-sequencing method by use of 28 redundant internal sequencing primers (*red triangles*). *b*, From the long PCR products, products of sufficient quantity and quality for PCR direct sequencing were amplified. NC = negative control without DNA template. *c*, Each exon 34′–specific primer was designed to have only 3 nt of exon 34′, to prevent erroneous amplification due to slippage.

represent the decreased expression of many TAF1 isoforms in the XDP neurons, because of its original neuron specificity of expression. Finally, to determine the complete structure of the isoform containing the 6 bp of exon 34′, full-length cloning from libraries consisting of cDNAs enriched in their 5′ ends[10] was performed. A single cDNA containing exon 34′ was successfully cloned (fig. 6), and this had the complete translation frame of the major form of *TAF1* with an insertion of two amino acid residues, alanine and lysine, in the carboxyl terminal kinase domain.

Discussion

SVA retrotransposon insertions are thought to be active in the human genome and to alter the expression level of adjacent genes that cause diseases, such as autosomal recessive hypercholesterolemia (ARH [MIM 605747])[14] and Fukuyama-type congenital muscular dystrophy (FCMD [MIM 607440]).[15] SVA insertion was found in the 3′ UTR region of the FCMD gene and in an intronic region of the ARH gene, which showed association with the reduced expression level of these genes. SVA retrotransposon has a high degree of GC content (~70%) and a large number of CpG sites (>150) in its nucleotide sequence, so that it is frequently hypermethylated in its insertion site. In fact, the present study demonstrated that the SVA retrotransposon was hypermethylated in genomic DNA from the caudate nucleus of the patient with XDP (fig. 7), which was also used in northern analysis, quantitative RT-PCR, and in situ hybridization. Such hypermethylated status and high GC content are able to affect dynamics of surrounding nucleotide sequence, such as the *cis*-regulatory element, so SVA insertions may reduce the expression level of adjacent genes. For instance, many large introns of eukaryotes often contain tissue-specific *cis*-regulatory elements, such as enhancers or silencers.[16–22] Intron 32, the largest intron of *TAF1* (29,932 bp), possibly contains a

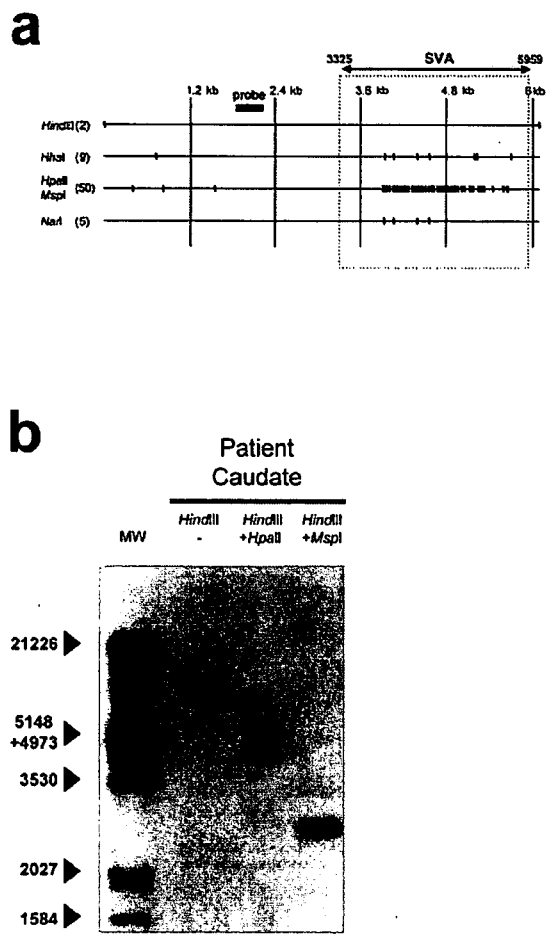

Figure 7. Detection of methylation around the SVA insertion. *a*, Restriction sites around the SVA insertion. The *Hind*III fragment and Southern probe are identical to those in figure 1*a*. The SVA insertion created 47 new *Hpa*II sites in the *Hind*III restriction fragment. *Msp*I is a CpG methylase-insensitive isoschizomer of *Hpa*II. *b*, Southern hybridization of genomic DNA from the patient's caudate. The 6.1-kb *Hind*III fragment was shifted, by additional *Hpa*II digestion, to an ~4.6-kb fragment. By contrast, the *Hind*III fragment was completely digested, by additional *Msp*I digestion, to a fragment of ~2.4 kb.

neuron-specific *cis*-regulatory element. Although involvement of other sequence variants in XDP pathogenesis is still possible, it is most likely that the SVA insertion impairs the function of a hypothetical neuron-specific *cis*-regulatory element, such as an enhancer, through changes in the methylation content and then substantially reduces the expressions of many isoforms of TAF1, including TA14-391, in the neurons. Because of the original neuron specificity of the expression, the TA14-391 isoform might represent the impairment more remarkably than do other isoforms. On the other hand, the remaining expression, as shown for TA14-391, despite being low, may compensate for complete loss of function and may account for the relatively late disease onset (age 39.5 ± 8.44 years) and the recessive mode of inheritance.

In summary, our results suggest that the SVA retrotransposon insertion into the *TAF1* gene may cause XDP by altering the expression of TAF1 isoforms, including TA14-391, possibly through DNA methylation changes. To our knowledge, our report is the first to reveal the entire genomic sequence of the *DYT3* region and to demonstrate at least one whole structure of the neuron-specific isoform of TAF1 and the disease-specific mutation, with a possible mechanism. To establish the disease specificity and the involvement mechanism of the SVA insertion in reduced expression of *TAF1* in XDP, further studies, such as an extensive population screening and genetic modification in model organisms, will be necessary and warranted. The TAF1 protein is the largest and the essential component of the TFIID complex in the pathway of RNA polymerase II–mediated gene transcription,[23,24] and it regulates transcription of a large number of genes related to cell division and proliferation.[23–25] How can a ubiquitous gene such as *TAF1* cause a disease that affects a selective part of the nervous system? We hypothesize that the neuron-specific isoforms and/or their enhanced expression level of *TAF1* (table 7) may play important roles in the nondividing cell. Sharing similar pathological features in the caudate nucleus, XDP and Huntington disease might result from disorders in the same biochemical pathway of RNA polymerase II–mediated gene transcription. In Huntington disease, for example, the abnormal huntingtin protein has been shown to interfere with the interaction between Sp1 and TAFII130, resulting in reduced expression of *DRD2* (MIM 126450) in the brain, including the caudate nucleus.[26] In XDP, the decreased expression of the TA14-391 isoform, and probably other TAF1 isoforms, may result in transcriptional dysregulation of many neuronal genes, including *DRD2*. We believe that the present findings in XDP support the concept of "transcription syndromes"[27] in TFIID, which include congenital cataracts facial dysmorphism neuropathy (CCFDN [MIM 604168]) syndrome, caused by a partial deficiency of RNA polymerase II[28]; Huntington disease[26]; dentato-rubro-pallidoluysian atrophy (DRPLA [MIM 125370]),[29] caused by interference in the signals to TFIID; and spinocerebellar ataxia 17 (SCA17 [MIM 607136]),[30] caused by an expanded polyglutamine in the TATA-binding protein (TBP [MIM 600075]).

Acknowledgments

We thank S. Fahn (Neurological Institute of New York, Columbia University) and M. Nakagawa (Kyoto Prefectural University of Medicine) for their critical reading of the manuscript. This study was partly supported by a Grant-in-Aid for Scientific Research on Priority Areas (C) "Medical Genome Science"; by Center of Excellence grant 16101J-1 from the Japanese Ministry of Education,

Science, Culture, and Sports; and by Grant-in-Aid for Dystonia Research from the National Center of Neurology and Psychiatry, Japan.

Web Resources

Accession numbers and URLs for data presented herein are as follows:

dbSNP, http://www.ncbi.nlm.nih.gov/SNP/ (for newly described SNPs *ss66974122, ss66974125, ss66974128, ss66974131, ss66974134, ss66974137, ss66974140, ss66974143, ss66974146, ss66974149, ss66974152,* and *ss66974155*)

DNA Databank of Japan (DDBJ), http://www.ddbj.nig.ac.jp/Welcome-e.html (for the complete genomic sequence of the *DYT3* region [accession number AB191243])

Online Mendelian Inheritance in Man (OMIM), http://www.ncbi.nlm.nih.gov/Omim/ (for XDP, Huntington disease, *TAF1*, ARH, FCMD, *DRD2*, CCFDN, DRPLA, SCA17, and TBP)

References

1. Lee LV, Pascasio FM, Fuentes FD, Viterbo GH (1976) Torsion dystonia in Panay, Philippines. Adv Neurol 14:137–151
2. Lee LV, Munoz EL, Tan KT, Reyes MT (2001) Sex linked recessive dystonia parkinsonism of Panay, Philippines (XDP). Mol Pathol 54:362–368
3. Fahn S, Bressman SB, Marsden CD (1998) Classification of dystonia. Adv Neurol 78:1–10
4. Goto S, Lee LV, Munoz EL, Tooyama I, Tamiya G, Makino S, Ando S, Dantes MB, Yamada K, Matusmoto S, et al (2005) Functional anatomy of the basal ganglia in X-linked recessive dystonia-parkinsonism. Ann Neurol 58:7–17
5. Waters CH, Faust PL, Powers J, Vinters H, Moskowitz C, Nygaard T, Hunt AL, Fahn S (1993) Neuropathology of lubag (X-linked dystonia parkinsonism). Mov Disord 8:387–390
6. Wilhelmsen KC, Weeks DE, Nygaard TG, Moskowitz CB, Rosales RL, dela Paz DC, Sobrevega EE, Fahn S, Gilliam TC (1991) Genetic mapping of "Lubag" (X-linked dystonia-parkinsonism) in a Filipino kindred to the pericentromeric region of the X chromosome. Ann Neurol 29:124–131
7. Haberhausen G, Schmitt I, Kohler A, Peters U, Rider S, Chelly J, Terwilliger JD, Monaco AP, Muller U (1995) Assignment of the dystonia-parkinsonism syndrome locus, DYT3, to a small region within a 1.8-Mb YAC contig of Xq13.1. Am J Hum Genet 57:644–650
8. Nemeth AH, Nolte D, Dunne E, Niemann S, Kostrzewa M, Peters U, Fraser E, Bochukova E, Butler R, Brown J, et al (1999) Refined linkage disequilibrium and physical mapping of the gene locus for X-linked dystonia-parkinsonism (DYT3). Genomics 60:320–329
9. Nolte D, Niemann S, Muller U (2003) Specific sequence changes in multiple transcript system DYT3 are associated with X-linked dystonia parkinsonism. Proc Natl Acad Sci USA 100:10347–10352
10. Maruyama K, Sugano S (1994) Oligo-capping: a simple method to replace the cap structure of eukaryotic mRNAs with oligoribonucleotides. Gene 138:171–174
11. Lee JT, Davidow LS, Warshawsky D (1999) Tsix, a gene antisense to Xist at the X-inactivation centre. Nat Genet 21: 400–404
12. Shen L, Wu LC, Sanlioglu S, Chen R, Mendoza AR, Dangel AW, Carroll MC, Zipf WB, Yu CY (1994) Structure and genetics of the partially duplicated gene RP located immediately upstream of the complement C4A and the C4B genes in the HLA class III region: molecular cloning, exon-intron structure, composite retroposon, and breakpoint of gene duplication. J Biol Chem 269:8466–8476
13. Ostertag EM, Goodier JL, Zhang Y, Kazazian HH Jr (2003) SVA elements are nonautonomous retrotransposons that cause disease in humans. Am J Hum Genet 73:1444–1451
14. Wilund KR, Yi M, Campagna F, Arca M, Zuliani G, Fellin R, Ho YK, Garcia JV, Hobbs HH, Cohen JC (2002) Molecular mechanisms of autosomal recessive hypercholesterolemia. Hum Mol Genet 11:3019–3030
15. Kobayashi K, Nakahori Y, Miyake M, Matsumura K, Kondo-Iida E, Nomura Y, Segawa M, Yoshioka M, Saito K, Osawa M, et al (1998) An ancient retrotransposal insertion causes Fukuyama-type congenital muscular dystrophy. Nature 394: 388–392
16. Gillies SD, Morrison SL, Oi VT, Tonegawa S (1983) A tissue-specific transcription enhancer element is located in the major intron of a rearranged immunoglobulin heavy chain gene. Cell 33:717–728
17. Halder G, Callaerts P, Gehring WJ (1995) Induction of ectopic eyes by targeted expression of the eyeless gene in *Drosophila*. Science 267:1788–1792
18. Dirksen WP, Mohamed SA, Fisher SA (2003) Splicing of a myosin phosphatase targeting subunit 1 alternative exon is regulated by intronic cis-elements and a novel bipartite exonic enhancer/silencer element. J Biol Chem 278:9722–9732
19. Donoghue M, Ernst H, Wentworth B, Nadal-Ginard B, Rosenthal N (1988) A muscle-specific enhancer is located at the 3′ end of the myosin light-chain 1/3 gene locus. Genes Dev 2:1779–1790
20. Annweiler A, Muller-Immergluck M, Wirth T (1992) Oct2 transactivation from a remote enhancer position requires a B-cell-restricted activity. Mol Cell Biol 12:3107–3116
21. Banerji J, Rusconi S, Schaffner W (1981) Expression of a beta-globin gene is enhanced by remote SV40 DNA sequences. Cell 27:299–308
22. Rippe RA, Lorenzen SI, Brenner DA, Breindl M (1989) Regulatory elements in the 5′-flanking region and the first intron contribute to transcriptional control of the mouse alpha 1 type I collagen gene. Mol Cell Biol 9:2224–2227
23. Hisatake K, Hasegawa S, Takada R, Nakatani Y, Horikoshi M, Roeder RG (1993) The p250 subunit of native TATA box-binding factor TFIID is the cell-cycle regulatory protein CCG1. Nature 362:179–181
24. Ruppert S, Wang EH, Tjian R (1993) Cloning and expression of human TAFII250: a TBP-associated factor implicated in cell-cycle regulation. Nature 362:175–179
25. Wassarman DA, Sauer F (2001) TAF(II)250: a transcription toolbox. J Cell Sci 114:2895–2902
26. Dunah AW, Jeong H, Griffin A, Kim YM, Standaert DG, Hersch SM, Mouradian MM, Young AB, Tanese N, Krainc D (2002) Sp1 and TAFII130 transcriptional activity disrupted in early Huntington's disease. Science 296:2238–2243
27. Vermeulen W, van Vuuren AJ, Chipoulet M, Schaeffer L, Appeldoorn E, Weeda G, Jaspers NG, Priestley A, Arlett CF, Lehmann AR, et al (1994) Three unusual repair deficiencies associated with transcription factor BTF2(TFIIH): evidence for the existence of a transcription syndrome. Cold Spring Harb Symp Quant Biol 59:317–329
28. Varon R, Gooding R, Steglich C, Marns L, Tang H, Angelicheva

D, Yong KK, Ambrugger P, Reinhold A, Morar B, et al (2003) Partial deficiency of the C-terminal-domain phosphatase of RNA polymerase II is associated with congenital cataracts facial dysmorphism neuropathy syndrome. Nat Genet 35:185–189

29. Igarashi S, Koide R, Shimohata T, Yamada M, Hayashi Y, Takano H, Date H, Oyake M, Sato T, Sato A, et al (1998) Suppression of aggregate formation and apoptosis by transglutaminase inhibitors in cells expressing truncated DRPLA protein with an expanded polyglutamine stretch. Nat Genet 18:111–117
30. Nakamura K, Jeong SY, Uchihara T, Anno M, Nagashima K, Nagashima T, Ikeda S, Tsuji S, Kanazawa I (2001) SCA17, a novel autosomal dominant cerebellar ataxia caused by an expanded polyglutamine in TATA-binding protein. Hum Mol Genet 10:1441–1448

Acta Neuropathol (2006) 111: 109–114
DOI 10.1007/s00401-005-0004-1

ORIGINAL PAPER

Hiroshige Fujishiro · Hiroyuki Umegaki
Daisuke Isojima · Hiroyasu Akatsu · Akihisa Iguchi
Kenji Kosaka

Depletion of cholinergic neurons in the nucleus of the medial septum and the vertical limb of the diagonal band in dementia with Lewy bodies

Received: 31 July 2005 / Revised: 19 September 2005 / Accepted: 19 September 2005 / Published online: 19 January 2006

Abstract The cholinergic basal forebrain is divided into four subregions (Ch1–4), and cholinergic neuronal loss in the nucleus basalis of Meynert (Ch4) has been correlated with cognitive impairments in both Alzheimer's disease (AD) and dementia with Lewy bodies (DLB). However, the Ch1–2 regions, which provide the major cholinergic innervation to the hippocampus, have not been investigated in DLB. The purpose of this study was to reveal the cholinergic neuronal changes in the medial septum (Ch1) and the nucleus of the vertical limb of the diagonal band (Ch2) of DLB brains. Using choline acetyltransferase (ChAT) immunohistochemistry, we showed that the number of ChAT-immunoreactive neurons in DLB brains was significantly lower than the numbers in AD and non-demented (control) brains. No significant difference in the number of ChAT-immunoreactive neurons was found between the AD and control brains. Moreover, the size of the ChAT-immunoreactive neurons was significantly smaller in the AD and DLB brains than in the control brains. These results show that cholinergic neurons of the Ch1-2 regions are more severely affected in DLB than in AD. Our DLB cases did not fulfill the neuropathologic criteria for definite AD. Furthermore, some Lewy bodies were observed in the Ch1-2 regions. Thus, cholinergic neuronal loss in the Ch1-2 regions might be specific to the pathology of DLB. Taking the distribution of cholinergic fibers in the hippocampus into consideration, this study suggests a possibility that hippocampal cholinergic projection is involved in Lewy-related neurites in the CA2–3 regions, the origin of which remains unclear.

Keywords Septal nuclei · Basal forebrain · Immunohistochemistry · Choline acetyltransferase · Cholinesterase inhibitor

H. Fujishiro (✉) · H. Umegaki · A. Iguchi
Department of Geriatrics, Medicine in Growth and Aging, Program in Health and Community Medicine, Nagoya University Graduate School of Medicine, 65 Tsurumai-cho, Showa-ku, 466-8550, Nagoya, Japan
E-mail: fujishi@med.nagoya-u.ac.jp

D. Isojima · H. Akatsu · H. Fujishiro
Choju Medical Institute, Fukushimura Hospital, 19-16 Noyori-cho, Aza-yamanaka, 441-8124, Toyohashi, Japan

K. Kosaka · D. Isojima
Department of Psychiatry, Yokohama City University, 3-9 Fukuura, Kanazawa-ku, 236-0004, Yokohama, Japan

Introduction

Dementia with Lewy bodies (DLB) is the second most frequent neurodegenerative dementing disorder after Alzheimer's disease (AD) [1, 18]. Hippocampal pathology is important in DLB as well as AD, since memory impairment, a chief symptom of both the disorders, is closely related to degeneration of the hippocampus. Lewy-related neurites are usually observed in the CA2–3 regions of the hippocampus in DLB [6, 7, 9, 11, 18], whereas these regions are relatively preserved in AD. In addition, immunoelectron microscopic examinations have revealed that these Lewy-related neurites are distal axons that have undergone change. These neurites are partially immunostained with a neurofilament antibody, but not with a tyrosine hydroxylase antibody [7]. Although the origin of Lewy-related neurites has been poorly understood, the absence of the degenerating axon terminals in hippocampal regions other than the CA2–3 regions of DLB brains might indicate that this pathology is associated with impairments of the hippocampal projection.

Cholinergic neurons in the basal forebrain form a cholinergic column comprising the medial septum, the nucleus of the diagonal band, and the nucleus basalis of Meynert. Mesulam et al. proposed the nomenclature of Ch1 through 4 to designate the various subdivisions of the basal forebrain cholinergic neurons [19]. The medial septum (Ch1) and the vertical limb of the nucleus of the diagonal band (Ch2) provide the cholinergic innervation of the hippocampal formation, and the nucleus basalis

(Ch4) projects to the amygdaloid nuclei and the cerebral cortex [15, 22]. Choline acetyltransferase (ChAT) activity in the cerebral cortex, a decrease in which is correlated with neuronal loss in the nucleus basalis of Meynert (Ch4), has been reported to be involved in cognitive function [16]. Moreover, the reduction of the neocortical presynaptic cholinergic inputs is more severe in DLB brains than in AD brains. Therefore, cholinesterase inhibitors are thought to be more effective in DLB patients than in AD patients [2, 10, 26]. On the other hand, cholinergic neurons within the hippocampal projecting nuclei of the Ch1–2 regions are minimally affected in AD brains as compared with non-demented brains [21, 23]. These neurons have not yet been investigated in DLB brains.

A previous study of ChAT-like immunoreactivity in hippocampal formation in humans showed that punctuate ChAT-immunostaining was conspicuous in the stratum pyramidale of the CA2–3 regions [27]. In the current study, we hypothesized that the Ch1–2 cholinergic neurons projecting to the hippocampus are involved in hippocampal CA2–3 pathology. To test this hypothesis, we performed a qualitative and semiquantitative ChAT-immunohistochemical analysis of cholinergic neurons over the entire length of the Ch1–2 regions of DLB brains, AD brains and non-demented control brains, and compared the results.

Materials and methods

Subjects

Fifteen autopsied brains from eight DLB cases (DLB group: mean age, 75.0 ± 12.6 years; mean brain weight, 1,200 ± 119 g), four AD cases (AD group: mean age, 83.5 ± 0.5 years; mean brain weight, 1,090 ± 43 g) and three non-demented control cases (control group: mean age, 83.3 ± 3.5 years; mean brain weight, 1,145 ± 123 g) were examined in the present study. DLB was diagnosed based on the neuropathological criteria of DLB and divided into five limbic types and three neocortical types [18]. Four AD cases fulfilled the neuropathological criteria of AD according to the NIA-RI-criteria [31]. The progression of Alzheimer pathology was classified from stages 1 to 6 by Braak staging [4]. Neither the DLB group nor the control group fulfilled the pathological criteria for AD [17, 31]. No significant difference was found in mean age or mean brain weight among the three groups. The mean values of the final mini-mental state examination (MMSE) cognitive score before death were also compared between the DLB group and AD group [8], and no significant difference was found (mean MMSE for the DLB group: 4.5 ± 4.7; for the AD group: 4.0 ± 8.0). Informed written consent was obtained from the patients' guardians before carrying out the dissection, and study design was approved by the ethics committee of the Choju medical institute.

Immunocytochemistry

Tissue blocks including the septal nucleus and the vertical limb of the diagonal band were fixed in 4% paraformaldehyde in 0.1 M phosphate buffer (pH 7.4), embedded in paraffin and cut into serial coronal 7-μm-thick sections. The region studied extended from the anterior border of the septal nucleus to the anterior commissure. Sections taken every 280 μm, i.e., every 40th section were stained with hematoxylin-eosin (HE). By this method, we could examine the entire medial septal nucleus and vertical limb of the diagonal band. After the limits were decided, serial sections (seven to ten sections for each brain) were pretreated with 0.1% trypsin diluted with 0.1% $CaCl_2$ for 20 min, and then immunostained with polyclonal goat anti-ChAT antibody (1:100; Chemicon, Temecula, CA, USA) and monoclonal mouse anti-phosphorylated α-synuclein antibody (1:1,000; Wako, Tokyo, Japan) overnight at 4°C. Alfa-synuclein-immunostaining was performed to confirm the presence of Lewy bodies in the Ch1–2 regions in cases where bodies were observed by HE staining. These primary antibodies were diluted with phosphate-buffered saline (PBS) containing 3% normal goat serum. After incubation with the primary antibodies, the sections were treated with biotinylated secondary antibodies for 2.5 h at room temperature, followed by incubation in avidin-biotinylated horseradish peroxidase (HRP) complex (ABC Elite Kit; Vector, Burlingame, CA, USA) for 0.5 h at room temperature. Immunolabeling was visualized with 3,3′-diaminobenzidine (DAB; Dojindo, Kumamoto, Japan) and nickel ammonium sulfate. Before α-synuclein immunostaining, sections were pretreated with 98% formic acid for 3 min. To investigate the AD pathology in the Ch1–2 regions, the sections from all the brains were also stained by the Gallyas–Braak method.

Semiquantitative analysis of ChAT-immunoreactive neurons

ChAT-immunoreactive neurons in the Ch1–2 regions were semiquantitatively analyzed to investigate the depletion of cholinergic neurons. The number of ChAT-immunoreactive neurons was counted on each section by the two investigators (H.F. and D.I.) who were blinded to the groups. The assessments were repeated and any discrepancies between the evaluations of the two raters were resolved through discussion. The numbers of ChAT-immunoreactive neurons on each of the serial sections at 280 μm intervals were summed, and this value served as a substitute for the total number of neurons in each case.

Densitometric analysis of ChAT-immunoreactive neurons

ChAT-immunoreactivity was investigated by densitometric analysis to detect the depletion of cholinergic

activity in each neuron. The sections were examined under an Olympus microscopy with Olympus AX80T at a total magnification of 200 times. All of the digital images of ChAT-immunoreactive neurons were converted to grayscale using Photoshop 4.0J image processing software (Adobe Systems, Tokyo, Japan) and the image analysis was performed using Scion Image Beta software, Version 4.02 (Scion, Frederick, MD, USA) to determine the pixel density of ChAT-positive cells at a given threshold level. In the present study, the pixel counts of the ChAT-positive neurons determined by image analysis served as a substitute for the cell surface measurement in each neuron. ChAT-immunoreactive neurons in the Ch2 region were randomly selected and the cell surface measurement was performed (pixels/cell). The average cell surface value was calculated for 100 neurons in each brain, followed by the average cell surface value for each of three groups.

Statistical analysis

The data are expressed as the mean ± SEM. The Kruskal–Wallis test followed by the Mann–Whitney *U*-test was used to compare differences among the three groups. p values below 0.05 were considered statistically significant. All statistical analysis was performed using StatView software (Version 5.0) for Windows.

Results

ChAT-immunoreactive neurons were observed from the medial septum (Ch1) to the nucleus of the vertical limb of the diagonal band (Ch2) in all cases. The Ch2 merges with the caudal portions of the Ch1; the Ch2 is located ventral to the decussation of the anterior commissure and reaches the posterior edge of the ventral striatum.

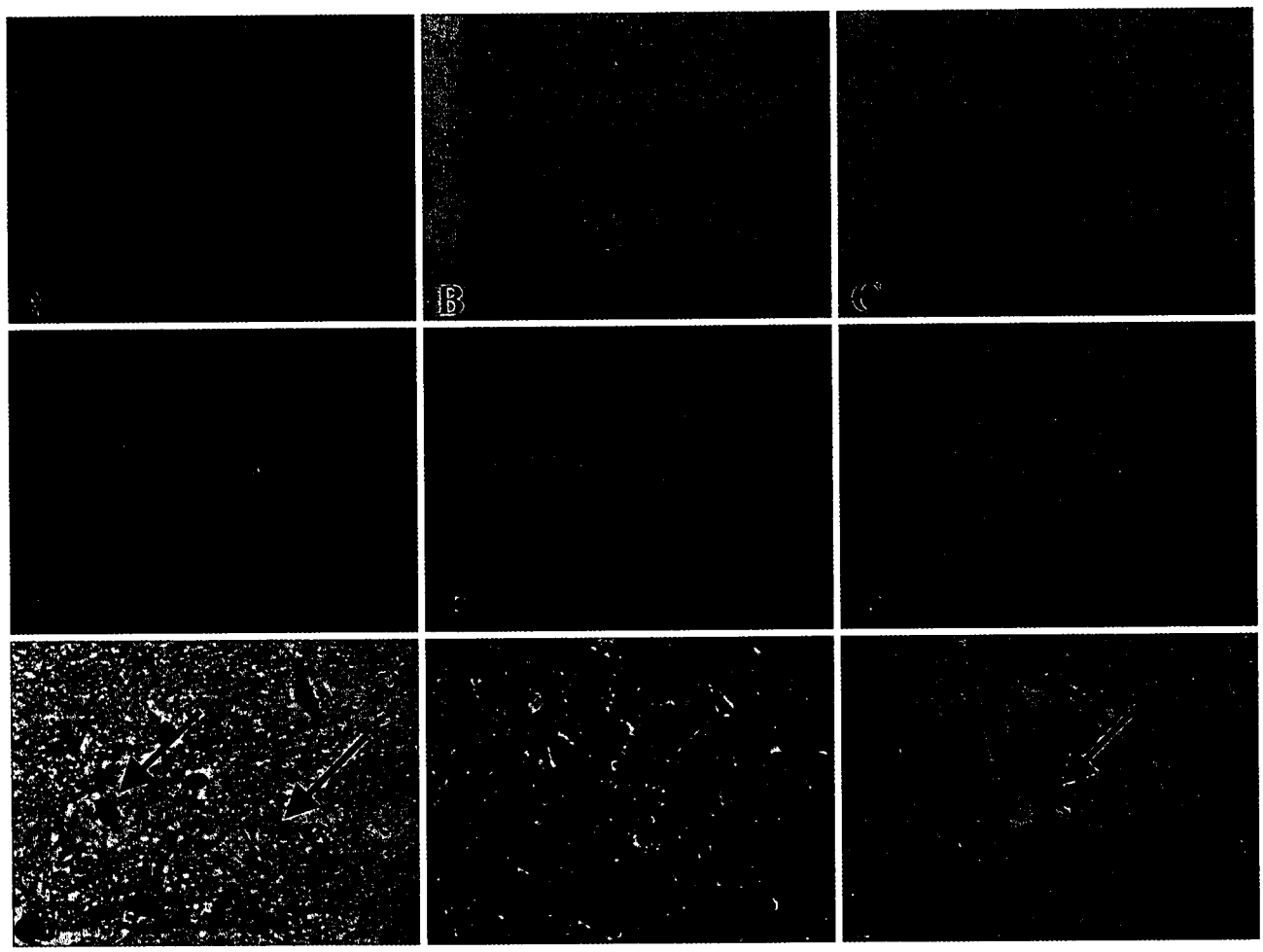

Fig. 1 **a** and **d** ChAT-immunoreactive neurons in the Ch1–2 regions of case 2 (non-demented). **b** and **e** ChAT-immunoreactive neurons in the Ch1–2 regions of case 4 (AD). **c** and **f** ChAT-immunoreactive neurons in the Ch1–2 regions of case 9 (DLB). ChAT immunostainings are shown at a total magnification of 100 times (**a–c**) or 200 times (**d–f**). **g** Neurofibrillary tangle (*NFT*) (*arrows*) in the Ch1–2 regions of the AD brain at a total magnification of 400 times by Gallyas–Braak staining. **h** and **i** Lewy bodies (*arrow*) in the Ch1–2 regions of the DLB brain at a total magnification of 400 times by HE staining and α-synuclein immunostaining

ChAT-immunoreactive neurons in the Ch1 region tend to be ovoid with vertical orientation, while most of those in the Ch2 region are fusiform-to-oval. In addition, the ChAT-immunoreactive neurons appeared to be sparser in the Ch1–2 regions of the DLB brains than in those of the AD and control brains (Fig. 1a–c). On the other hand, the degree of immunostaining was variable, ranging from light to strong in all cases (Fig. 1d–f).

When Alzheimer pathology was examined according to Braak staging [4], the control cases and most of the DLB cases were found to be in Braak stages 1–3 (Table 1). These findings did not fulfill the neuropathologic criteria for definite AD. Moreover, neurofibrillary tangles were observed in the Ch2 region of all the AD cases by using the Gallyas–Braak staining method, but were not found in the Ch2 region of the DLB and control cases (Fig. 1g). On the other hand, Lewy bodies were observed in the Ch1–2 regions of the DLB group (Fig. 1h, i).

ChAT-immunostaining revealed cholinergic neuronal changes in the Ch1–2 regions of the DLB brains. Significant differences among the three groups were found in both the number and the mean surface area of the ChAT-immunoreactive neurons projecting to the hippocampus (each $p < 0.05$, Kruskal–Wallis test). The number of these neurons was significantly reduced in the DLB group compared with the AD and control groups (each $p < 0.05$, Mann–Whitney *U*-test). No significant difference was found in the number of the ChAT-immunoreactive neurons between the AD and control groups, as expected from the previous studies [21, 23] (Fig. 2). On the other hand, when densitometric analysis of ChAT-immunoreactive neurons was performed, the mean surface areas of the AD and DLB groups were significantly reduced compared with the control group (each $p < 0.05$, Mann–Whitney *U*-test). No significant difference was found in the mean surface area of the ChAT-immunoreactive neurons between the AD and DLB groups (Fig. 3).

Discussion

In this study, we found that the cholinergic neurons projecting to the hippocampus were notably degenerated in the DLB group compared with the AD and control groups. However, no significant difference was found in the number of the ChAT-immunoreactive neurons between the AD and control groups, in agreement with the previous reports [21, 23]. Moreover, the mean surface area of ChAT-immunoreactive neurons in the AD and DLB groups was significantly reduced as compared with that in the control group. Based on the fact that atrophy of basal forebrain neurons occurs with the degenerative processes in AD [25, 29], our study showed that cholinergic neurons in the Ch1–2 regions of the AD group were relatively spared in comparison with those of the DLB group. Curiously, a previous volumetry study based on MR imaging supports our results: Brenneis et al. reported that the atrophy of the basal forebrain, including the Ch1–2 regions, of patients with DLB was significantly greater than that of patients with AD [3]. Because Lewy pathology, but not AD pathology, was observed in the Ch1–2 regions of all the DLB cases in the present study, cholinergic neuronal degeneration in the Ch1–2 regions might be specific to the pathogenesis of DLB.

The major cholinergic input to the hippocampus enters the structure via the fimbria-fornix, and the distribution of cholinergic fibers and terminals in the

Table 1 Clinical and pathological data of our cases

	Age (years)	Sex	Brain wt. (g)	Braak stage (NFT)	Duration of Illness	Cause of death
Control (non-demented)						
1	87	F	1015	2	–	Pancreas cancer
2	80	M	1260	1	–	Prostate cancer, heart failure
3	83	F	1160	2	–	Acute cardiomyocarditis
Alzheimer's disease (*AD*)						
4	84	M	1140	5	3	Pneumonia
5	83	F	1040	6	6	Gastric cancer
6	84	F	1070	5	15	Gastric cancer
7	83	M	1110	5	7	Pneumonia
Dementia with Lewy bodies (*DLB*)						
8	47	F	1060	0[a]	4	Heart failure
9	82	M	1150	3	3	Pneumonia
10	79	M	1300	3	3	Pneumonia
11	69	M	1240	3	3	Pneumonia
12	85	F	1010	3	9	Heart failure
13	72	M	1350	1	4	Pneumonia
14	84	M	1200	2	7	Pneumonia
15	82	F	1290	2	4	Pneumonia

[a]No NFT in the brain

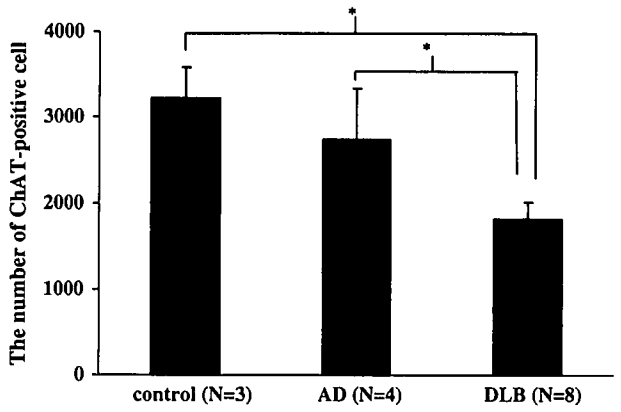

Fig. 2 The number of ChAT-positive neurons projecting to the hippocampus in each group. $*p < 0.05$

hippocampus has been reported [14]. Curiously, a previous study showed that punctate ChAT-immunostaining was conspicuous in the stratum pyramidale of the CA2–3 area, and that the highest density of ChAT-positive terminals was found in the stratum pyramidale and the juxtrapyramidal zone of the stratum oriens [27]. Another immunostaining study revealed that nerve growth factor (NGF), which plays an important role in sustaining and surviving cholinergic neurons, is mainly localized within the CA2–4 area, but is not present in the CA1 or subiculum [24]. On the other hand, Lewy-related neurites in the DLB brains are specific to the CA2–3 area in the hippocampus. In addition, ultrastructural and immunohistochemical studies suggest that these neurites are abnormal axon terminals. These findings lead us to conjecture that the depletion of cholinergic neurons projecting to the hippocampus in the DLB brain can be attributed to the Lewy-related neurites of the CA2–3 area. However, we did not investigate the ChAT-immunoreactivity of Lewy-related neurites in the present study, and thus, further studies will be needed to clarify the origin of Lewy-related neurites in the CA2–3.

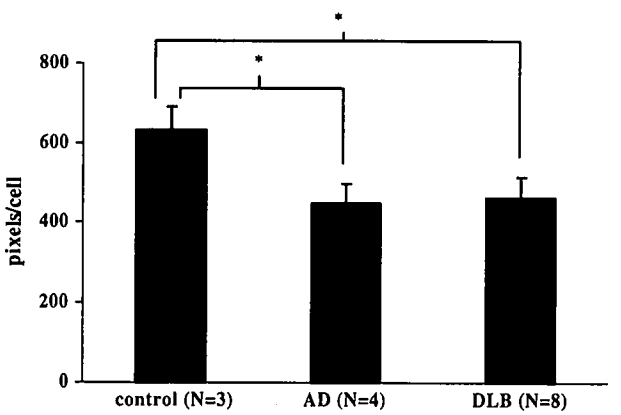

Fig. 3 The mean surface area (pixels/cell) of ChAT-positive neurons in each group. $*p < 0.05$

There have been several animal studies on immunotoxic lesions that specifically damage the cholinergic neurons projecting to the hippocampus. For example, monkeys with damages to the cholinergic neurons projecting to the hippocampus showed impaired performance on visual-spatial conditional learning tasks [28]. Moreover, rats with similar damages to cholinergic neurons showed impaired performance on environment-spatial conditional learning tasks [12]. These results may indicate that cholinergic neurons projecting to the hippocampus participate in certain visual-spatial cognitive impairments specific to DLB patients [5, 20].

Some clinical trials have reported that cholinesterase inhibitors are more effective in DLB patients than in AD patients [13, 30]. Treatment with these agents has positive effects on cognitive impairments, psychiatric symptoms, and global dysfunction. Visual hallucination, which is one of the three core clinical features in DLB, is also improved by cholinesterase inhibitors. From a clinical point of view, the severe depletion of cholinergic neurons projecting to the hippocampus in DLB might provide grounds for pharmacological intervention with cholinesterase inhibitors.

Reference

1. Akatsu H, Takahashi M, Matsukawa N, Ishikawa Y, Kondo N, Sato T, Nakazawa H, Yamada T, Okada H, Yamamoto T, Kosaka K (2002) Subtype analysis of neuropathologically diagnosed patients in a Japanese geriatric hospital. J Neurol Sci 196:63–69
2. Bohnen NI, Kaufer DI, Ivanco LS, Koeppe RA, Davis JG, Mathis CA, Moore RY, DeKosky ST (2003) Cortical cholinergic function is more severely affected in parkinsonian dementia than in Alzheimer disease: an in vivo positron emission tomographic study. Arch Neurol 60:1745–1748
3. Brenneis C, Wenning GK, Egger KE, Schocke M, Trieb T, Seppi K, Marksteiner J, Ransmayr G, Benke T, Poewe W (2004) Basal forebrain atrophy is a distinctive pattern in dementia with Lewy bodies. Neuroreport 15:1711–1714
4. Braak H, Braak E (1991) Neuropathological stageing of Alzheimer-related changes. Acta Neuropathol 82:239–259
5. Collerton D, Burn D, McKeith I, O'Brien J (2003) Systematic review and meta-analysis show that dementia with Lewy bodies is a visual-perceptual and attentional-executive dementia. Dement Geriatr Cogn Disord 16:229–237
6. Dickson DW, Ruan D, Crystal H, Mark MH, Davies P, Kress Y, Yen S-H (1991) Hippocampal degeneration differentiates diffuse Lewy body disease (DLBD) from Alzheimer's disease: light and electron microscopic immunocytochemistry of CA2-3 neurites specific to DLBD. Neurology 41:1402–1409
7. Dickson DW, Schmidt ML, Lee VM-Y, Zhao M-L, Yen S-H, Trojanowski JQ (1994) Immnoreactivity profile of hippocampal CA2/3 neurites in diffuse Lewy body disease. Acta Neuropathol 87:269–276
8. Folstein M, Folstein SE, McHugh PR (1975) Mini-mental state. A practical method for grading the cognitive state of patients for the clinician. J Psychiatr Res 12:189–198
9. Galvin JE, Uryu K, Lee VM-Y, Trojanowski JQ (1999) Axon pathology in Parkinson's disease and Lewy body dementia hippocampus contains α-, β-, and γ-synuclein. Proc Natl Acad Sci USA 96:13450–13455
10. Iraizoz I, Guijarro JL, Gonzalo LM, De Lacalle S (1999) Neuropathological changes in the nucleus basalis correlate with clinical measures of dementia. Acta Neuropathol 98:186–196

11. Iseki E, Li F, Odawara T, Kosaka K (1997) Hippocampal pathology in diffuse Lewy body disease using ubiquitin immunohistochemistry. J Neurol Sci 149:165–169
12. Janisiezka AM, Jackson O III, Firoz EF, Baxter MG (2004) Environment-spatial conditional learning in rats with selective lesions of medial septal cholinergic neurons. Hippocampus 14:265–273
13. Kaufer DI (2004) Pharmacologic treatment expectations in the management of dementia with Lewy bodies. Dement Geriatr Cogn Disord 17:32–39
14. Kitt CA, Mitchell SJ, Delong MR, Wainer BH, Price DL (1987) Fiber pathways of basal forebrain cholinergic neurons in monkeys. Brain Res 406:192–206
15. Kordower JH, Gash DM, Bothwell M, Hersh L, Mufson EJ (1989) Nerve growth factor and choline acetyltransferase remain colocalized in the nucleus basalis (Ch4) of Alzheimer's disease patients. Neurobiol Aging 10:287–294
16. Lippa CF, Smith TW, Perry E (1999) Dementia with Lewy bodies: choline acetyltransferase parallels nucleus basalis pathology. J Neural Transm 106:525–535
17. Marui W, Iseki E, Kato M, Akatsu H, Kosaka K (2004) Pathological entity of dementia with Lewy bodies and its differentiation from Alzheimer's disease. Acta Neuropathol 108:121–128
18. McKeith IG, Galasko D, Kosaka K, Perry EK, Dickson DW, Hansen LA, Salmon DP, Lowe J, Mirra SS, Byrne EJ, Lennox G, Quinn NP, Edwardson JA, Ince PG, Bergeron C, Burns A, Miller BL, Lovestone S, Collerton D, Jansen ENH, Ballard C, de Vos RAI, Wilcock GK, Jellinger KA, Perry RH (1996) Consensus guidelines for the clinical and pathologic diagnosis of dementia with Lewy bodies (DLB). Neurology 47:1113–1124
19. Mesulam M-M, Mufson EJ, Levey AI, Wainer BH (1983) Cholinergic innervation of cortex by the basal forebrain: cytochemistry and cortical connections of the septal area, diagonal band nuclei, nucleus basalis (substantia innominata) and hypothalamus in the rhesus monkey. J Comp Neurol 214:170–197
20. Mori E, Shimomura T, Fujimori M, Hirono N, Imamura T, Hashimoto M, Tanimukai S, Kazui H, Hanihara T (2000) Visuoperceptual impairment in Dementia with Lewy bodies. Arch Neurol 57:489–493
21. Mufson EJ, Bothwell M, Kordower JH (1989) Loss of nerve growth factor receptor-containing neurons in Alzheimer's disease: a quantitative analysis across subregions of the basal forebrain. Exp Neurol 105:221–232
22. Mufson EJ, Bothwell M, Hersh LB, Kordower JH (1989) Nerve growth factor receptor immunoreactive profiles in the normal, aged human basal forebrain: colocalization with cholinergic neurons. J Comp Neurol 285:196–217
23. Mufson EJ, Cochran E, Benzing W, Kordower JH (1993) Galaninergic innervation of the cholinergic vertical limb of the diagonal band (Ch2) and bed nucleus of the stria terminalis in aging, Alzheimer's disease and down's syndrome. Dementia 4:237–250
24. Mufson EJ, Conner JM, Varon S, Kordower JH (1994) Nerve growth factor-like immunoreactive profiles in the primate basal forebrain and hippocampal formation. J Comp Neurol 341:507–519
25. Pearson RCA, Sofroniew MV, Cuello AC, Powell TPS, Eckenstein F, Esiri MM, Wilcock GK (1983) Persistence of cholinergic neurons in the basal nucleus in a brain with senile dementia of the Alzheimer's type demonstrated by immunohistochemical staining for choline acetyltransferase. Brain Res 289:375–379
26. Perry EK, Irving D, Kerwin JM, McKeith IG, Thompson P, Collerton D, Fairbairn AF, Ince PG, Morris CM, Cheng AV, Perry RH (1993) Cholinergic transmitter and neurotrophic activities in Lewy body dementia: similarity to Parkinson's and distinction from Alzheimer disease. Alzheimer Dis Assoc Disord 7:69–79
27. Ransmayr G, Cervera P, Hirsch E, Ruberg M, Hersh LB, Duyckaerts C, Hauw J-J, Delumeau C, Agid Y (1989) Choline acetyltransferase-like immunoreactivity in the hippocampal formation of control subjects and patients with Alzheimer's disease. Neuroscience 32:701–714
28. Ridley RM, Barefoot HC, Maclean CJ, Pugh P, Baker HF (1999) Different effects on learning ability after injection of the cholinergic immunotoxin ME20. 4IgG-saporin into the diagonal band of Broca, basal nucleus of Meynert, or both in monkeys. Behav Neurosci 113:303–315
29. Rinne JO, Paljarvi L, Rinne UK (1987) Neuronal size and density in the nucleus basalis of Meynert in Alzheimer's disease. J Neurol Sci 79:67–76
30. Tirabosci P, Hansen LA, Alford M, Sabbagh MN, Schoos B, Masliah E, Thal LJ, Corey-Bloom J (2000) Cholinergic dysfunction in disease with Lewy bodies. Neurology 54:407–411
31. The national institute on aging, reagan institute working group on diagnostic criteria for the neuropathological assessment of Alzheimer's disease (1997) Consensus recommendations for the postmortem diagnosis of Alzheimer's disease. Neurobiol Aging 18:S1–S2